Emergent dynamics of adult stem cell lineages from single nucleus and single cell RNA-Seq of *Drosophila* testes

Amelie A. Raz[1#], Gabriela S. Vida[2#], Sarah R. Stern[3#], Sharvani Mahadevaraju[4#], Jaclyn M. Fingerhut[1#], Jennifer M. Viveiros[5#], Soumitra Pal[6#], Jasmine R. Grey[5#], Mara R. Grace[5#], Cameron W. Berry[3], Hongjie Li[7], Jasper Janssens[8], Wouter Saelens[9], Zhantao Shao[10], Chun Hun[10], Yukiko M. Yamashita[1], Teresa M. Przytycka[6], Brian Oliver[4], Julie A. Brill[11,12,13], Henry M. Krause[10,12], Erika L. Matunis[5], Helen White-Cooper[14], Stephen DiNardo[2]*, and Margaret T. Fuller[3,15]*

[1]Whitehead Institute for Biomedical Research and Department of Biology, Massachusetts Institute of Technology; Howard Hughes Medical Institute, Cambridge, MA 02139, USA
[2]Department of Cell and Developmental Biology, The Perelman School of Medicine and The Penn Institute for Regenerative Medicine, Philadelphia, PA 19104, USA.
[3]Department of Developmental Biology, Stanford University School of Medicine, Stanford, CA 94305 USA.
[4]National Institute of Diabetes and Digestive and Kidney Diseases, National Institutes of Health, Bethesda, MD 20814, USA.
[5]Department of Cell Biology, Johns Hopkins University School of Medicine, 725 N. Wolfe Street, Baltimore, MD 21205, USA.
[6]National Center for Biotechnology Information, National Library of Medicine, National Institutes of Health, Bethesda, MD 20894, USA.
[7]Huffington Center on Aging and Department of Molecular and Human Genetics, Baylor College of Medicine, Houston, TX 77030, USA.
[8]JVIB Center for Brain & Disease Research, and the Department of Human Genetics, KU Leuven, Leuven, Belgium.
[9]Data Mining and Modeling for Biomedicine, VIB Center for Inflammation Research, and Department of Applied Mathematics, Computer Science and Statistics, Ghent University, Ghent, Belgium.
[10]Donnelly Centre for Cellular and Biomolecular Research, University of Toronto, Toronto, Ontario M5S 3E1, Canada.
[11]Cell Biology Program, The Hospital for Sick Children, Toronto, Ontario M5G 0A4, Canada.
[12]Department of Molecular Genetics, University of Toronto, Toronto, Ontario M5S 1A8, Canada.
[13]Institute of Medical Science, University of Toronto, Toronto, Ontario M5S 1A8, Canada.
[14]School of Biosciences, Cardiff University, Museum Avenue, Cardiff, CF10 3AT, UK.
[15]Department of Genetics, Stanford University School of Medicine, Stanford, CA 94305 USA.

*Correspondence to:

sdinardo@pennmedicine.upenn.edu ORC ID: 0000-0003-4131-5511

and

mtfuller@stanford.edu ORC ID: 0000-0002-3804-4987

#contributed equally

Running title: adult fly testis atlas

Key words: stem cell / lineage / spermatogenesis / snRNA-seq / scRNA-seq

Abstract

Proper differentiation of sperm from germline stem cells, essential for production of the next generation, requires dramatic changes in gene expression that drive remodeling of almost all cellular components, from chromatin to organelles to cell shape itself. Here we provide a single nucleus and single cell RNA-seq resource covering all of spermatogenesis in *Drosophila* starting from in-depth analysis of adult testis single nucleus RNA-seq (snRNA-seq) data from the Fly Cell Atlas (FCA) study (Li *et al.*, 2022). With over 44,000 nuclei and 6,000 cells analyzed, the data provide identification of rare cell types, mapping of intermediate steps in differentiation, and the potential to identify new factors impacting fertility or controlling differentiation of germline and supporting somatic cells. We justify assignment of key germline and somatic cell types using combinations of known markers, *in situ* hybridization, and analysis of extant protein traps. Comparison of single cell and single nucleus datasets proved particularly revealing of dynamic developmental transitions in germline differentiation. To complement the web-based portals for data analysis hosted by the FCA, we provide datasets compatible with commonly used software such as Seurat and Monocle. The foundation provided here will enable communities studying spermatogenesis to interrogate the datasets to identify candidate genes to test for function *in vivo*.

Introduction

Single cell RNA-seq (scRNA-seq) of developing tissues can reveal new cell types as well as previously unknown steps in the differentiation of lineages underlying tissue homeostasis and repair. In fact, high-resolution expression maps are being created for entire organisms, from *C. elegans*, planaria, and schistosomes to *Drosophila* and mouse (Cao et al., 2017, 2019; Fincher et al., 2018; Li et al., 2022; Plass et al., 2018; Schaum et al., 2018; Sebé-Pedrós et al., 2018; Siebert et al., 2019; Wendt et al., 2020), with such atlases providing a foundational reference for several important model organisms. In particular, for tissues maintained by stem cell lineages, scRNA-seq can identify the developmental trajectories that lead from dedicated tissue stem cell to terminally differentiated cell types, an important resource for understanding tissue maintenance, repair, and the origins of cancer.

The testis harbors a highly active, unipotent adult stem cell lineage that must produce sperm throughout reproductive life. Spermatogenesis relies on self-renewing germline stem cells, the progeny of which differentiate into one of the most highly specialized cell types in the body. Production of functional sperm requires intimate interactions between germ cells and somatic support cells, with defects at almost any step compromising fertility. Interest in spermatogenesis has motivated scRNA-seq analyses of testes from a variety of organisms, including mouse (Cao et al., 2021; Chen et al., 2018; Green et al., 2018; Guo et al., 2020; Law et al., 2019) and *Drosophila* (Li et al., 2022; Mahadevaraju et al., 2021; Witt et al., 2019). Notably, the testis of *Drosophila* has the highest complexity in terms of mRNAs expressed of any tissue in the fly, likely reflecting the dramatic differentiation events required (Li et al., 2022).

Many aspects of spermatogenesis are conserved from *Drosophila* to mammals. One striking difference, however, is that spermatogenesis in *Drosophila* relies on not one but two adult stem cell lineages. The co-differentiating germ cells and their closely associated somatic support cells descend from distinct stem cell populations, housed together in a well-defined niche (Fuller, 1998). Additionally, the many mutations affecting male fertility, plus powerful genetic tools for cell type specific functional analysis, have allowed identification of stage-specific regulatory factors underlying niche function in stem cell maintenance, control of proliferation, and soma-germline feedback circuits that act during co-differentiation of these two lineages. This comprehensive

98 knowledge of spermatogenesis offers a rich biological foundation for interpreting single nucleus
99 and single cell RNA-seq data.

100 Here we present an in-depth analysis of the testis subset of the Fly Cell Atlas (FCA) single
101 nucleus RNA-Seq (snRNA-seq) data. We supplement this with scRNA-seq from the same tissue,
102 together providing a foundational reference for the field. While several recent RNA-seq analyses
103 of *Drosophila* testes have been illuminating, they generally focused on particular stages (Gan et
104 al., 2010; Hof-Michel and Bökel, 2020; Lu et al., 2020; Mahadevaraju et al., 2021; Shi et al., 2020;
105 Vedelek et al., 2018; Witt et al., 2019). In contrast, the scale and comprehensive nature of the
106 FCA dataset allowed us to profile rare cell types, such as the stem cell niche, and to follow
107 spermatogenesis from early spermatogonia to late spermatids, a remarkable conversion of
108 precursors to highly elongated, specialized cells. We present supporting data for assignment of
109 key cell types, both germline and somatic, and show how progression through two distinct, yet
110 intimately interacting, stem cell-based lineages emerges from the changes in gene expression.

111 The data confirm and extend known features of the male germ line transcription program,
112 including cell type specific expression of many genes in spermatocytes, downregulation of X-
113 linked genes in later spermatocytes, and repression of most transcription in early spermatids. At
114 the same time, surprising new features emerged, including unexpected complexity in the somatic
115 support cell lineage. In addition, comparison of single nucleus with single cell sequencing data
116 significantly expanded our understanding of gene expression dynamics in spermatocytes and
117 spermatids as they mature. In particular, these data showed how dynamic changes in active
118 transcription reflected in the snRNA-seq can be obscured by the endowment of mRNAs stored in
119 the cytoplasm. This is especially clear in early haploid spermatids, which have little transcriptional
120 activity but contain many mRNAs transcribed in spermatocytes and stored to be translated later
121 to support spermatid morphogenesis. With a gene expression framework for the two testis stem
122 cell lineages now in place, mining the snRNA-seq data for changes in gene expression as one
123 cluster advances to the next should identify new sub-stage-specific markers, thereby opening the
124 way for tests of function for such newly identified genes in male germ cell differentiation.

125

Results

Clustering by gene expression signature reveals progression of differentiation in two stem cell lineages

Spermatogenesis in *Drosophila* involves obligate, intimate interactions between cells differentiating in two adult stem cell-founded lineages. Male germline stem cells (GSCs) and their partners, the somatic cyst stem cells (CySCs), are both physically anchored to a small cluster of somatic cells termed the apical hub (Figure 1A), which provides short-range niche signals important for maintenance of the two stem cell states. The interleaved arrangement of GSCs and CySCs ensures that their immediate daughters are positioned to interact. Two postmitotic early cyst cells enclose each gonialblast (immediate GSC daughter), forming a two-cell squamous epithelium that soon seals the progeny of the gonialblast off from the rest of the testis (Fairchild et al., 2015). The gonialblast initiates four rounds of spermatogonial transit amplifying divisions with incomplete cytokinesis, producing 16 interconnected germ cells (Figure 1A). After the fourth mitosis, the germ cells undergo premeiotic S-phase and enter an extended G2 cell cycle phase termed meiotic prophase. Over the next three and a half days the 16 primary spermatocytes increase 25-fold in volume, engaging in a robust transcription program in preparation for the meiotic divisions and the extensive elongation and remodeling of the resulting 64 haploid spermatids into mature sperm. Although they do not divide, the two somatic cyst cells co-differentiate with the germ cells they enclose (Gönczy et al., 1992), eventually taking on different identities as head and tail cyst cells. The head cyst cell cups the nuclear end of elongating spermatid bundles and eventually inserts into the terminal epithelium at the base of the testis, while the tail cyst cell elongates extensively to cover the rest of the spermatid bundle (Tokuyasu et al., 1972). All these cell types, as well as somatic structural cells of the testis sheath (muscle and pigment cells) and cells of the seminal vesicle are represented in the FCA testis dataset.

The relative similarity and differences in gene expression for 44,621 single nuclei from triplicate 10X snRNA-seq runs from adult testis plus seminal vesicle (See Materials and Methods) can be visualized in a Uniform Manifold Approximation and Projection (UMAP)-based dimensionality reduction plot (Figure 1B). The geography of the UMAP is dominated by the

Figure 1

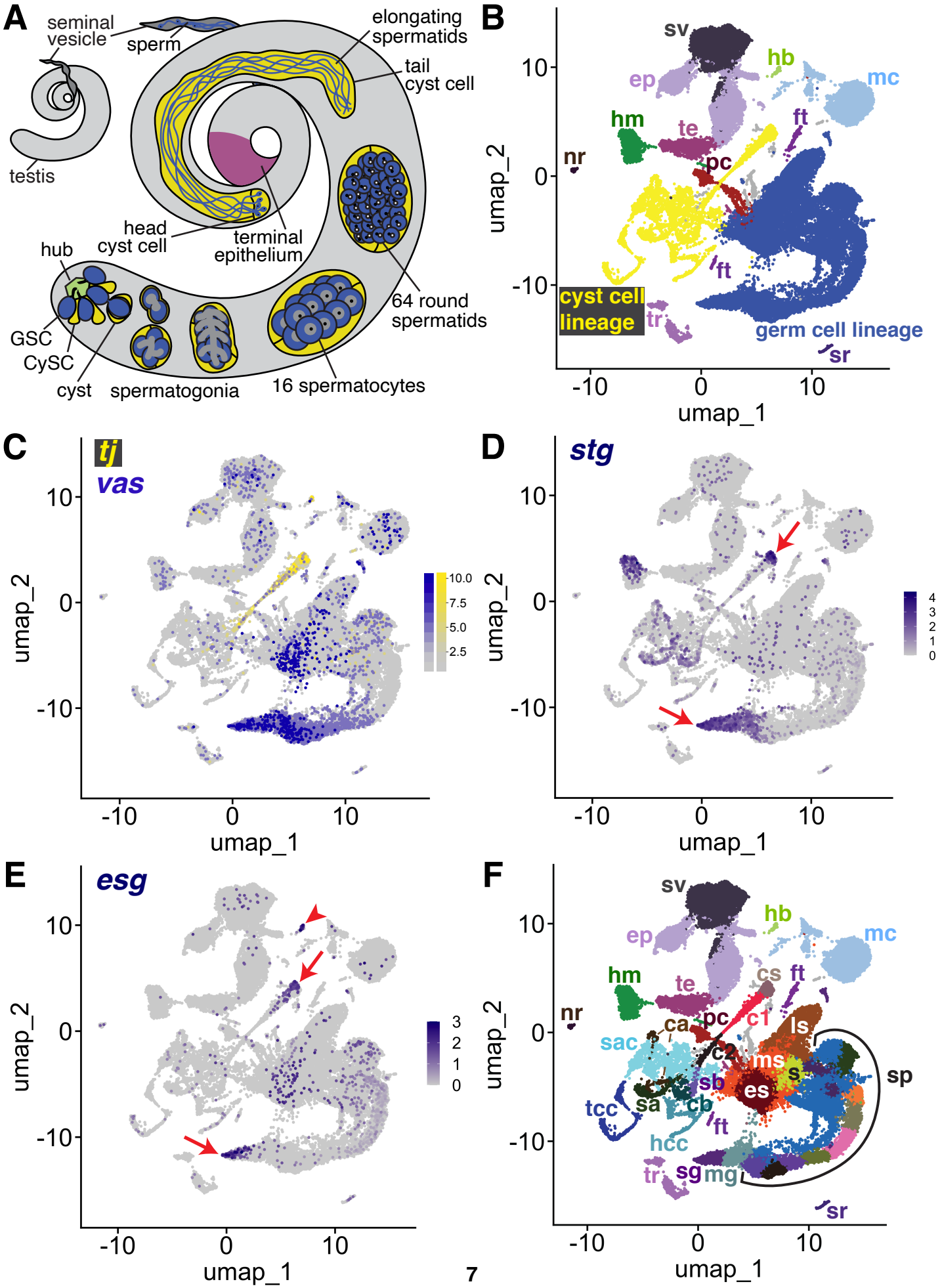

Figure 1

The snRNA-seq landscape of the testis

A) Illustration of adult *Drosophila* testis showing hub (green), germ cell lineage (blue), cyst cell lineage (yellow), terminal epithelium (pink) and seminal vesicle (gray). **B)** UMAP of FCA snRNA-seq data from the testis plus seminal vesicle (relaxed version). Blue: germ cell lineage; Yellow: cyst cell lineage; Pink: terminal epithelial cells of testis (te); Dark gray: seminal vesicle (sv). Other cell types as listed in **F**. **(C-E**) UMAP plots of snRNA-seq data showing expression of: **C)** *traffic jam* (*tj*) (yellow) and *vasa* (*vas*) (blue), **D)** *string* (*stg*), **E)** *escargot* (*esg*). Red arrows: proliferating cells, red arrowhead: hub. **F)** UMAP (as in **B**) with Leiden 6.0 clusters of germ and cyst cell lineages labeled (sg: Spermatogonium; mg: Mid-late proliferating spermatogonia; sp: Spermatocytes; s: Spermatids; es: Early elongation-stage spermatids; ms: Early-mid elongation-stage spermatids; ls: Mid-late elongation-stage spermatids; hb: Germinal proliferation center hub; cs: Cyst stem cell, c1: Early cyst cell 1; c2: Early cyst cell 2; sa: Cyst cell with spermatocytes branch A; sb: Cyst cell with spermatocytes branch B; ca: Cyst cell branch a; cb: Cyst cell branch b; sac: Elongating spermatid-associated cyst cell; hcc: Head cyst cell; tcc: Tail cyst cell; te: Terminal epithelial cells of testis; sv: Seminal vesicle; ep: Male gonad associated epithelium; sr: Secretory cells of the male reproductive tract; mc: Muscle cell; hm: Hemocyte; nr: Neuron; pc: Pigment cell;, tr: Trachea; ft: Fat body).

dynamic sequences of differentiating states in the germline (blue) and somatic cyst cell (yellow) lineages. Each lineage manifests as an emergent trajectory of nuclei with continuously progressing gene expression profiles, unlike the discrete clusters characteristic of most terminally differentiated cell types. Despite their physical proximity and cooperation *in vivo*, the germ line and cyst cell lineages mapped to largely non-overlapping formations in gene expression space represented in the UMAP, consistent with their different embryological origin, cell biology, and known roles.

From the perspective in Figure 1B, the spatial arrangement of nuclei in the UMAP whimsically resembles a hammerhead shark (blue - germ line) playing a saxophone (yellow - cyst cell lineage) watched over by a mermaid (several somatic epithelial-based structural elements, including the seminal vesicle (sv, dark purple) and terminal epithelial cells at the testis base (te, pink)). One notable cluster located near the mermaid head is the hub (hb, light green), the niche that supports the two stem cell lineages. Other clusters on the UMAP contain differentiated cell types that contribute to organ structure, including muscle (mc) and pigment cells (pc) of the testis sheath (Figure 1B). Additionally, sample dissection carried over small numbers of non-testis cells, including tracheal (tr) and fat body (ft) cells, hemocytes (hm), neurons (nr), and male reproductive tract secretory cells (sr).

Identity of key clusters was assigned based on expression of known markers from the literature (citations for all published markers employed given in Table 1). Expression of *vasa (vas)* identified early germ line nuclei while expression of *traffic jam (tj)* identified nuclei from early stages in the somatic cyst cell lineage (Figure 1C). Expression of the cdc25 phosphatase *string (stg)*, required for the G2/M transition in mitotic cells (Alphey et al., 1992; Edgar and O'Farrell, 1990), and *escargot (esg)*, a gene expressed in diploid proliferative cells (Fuse et al., 1994), marked CySCs in the cyst cell lineage and proliferating GSCs and spermatogonia in the germ line lineage (Figure 1D,E). Expression of *esg* also marked the hub, as expected from prior studies (Voog et al., 2014) (Figure 1E). Together, these markers established that the germ line lineage begins at the tail end of the "shark" with germ line stem cells (GSCs) and proliferating spermatogonia at the tapered point. The somatic cyst cell lineage begins at the mouthpiece of

TABLE 1:	List of genes used as markers in identifying key clusters			
Gene_symbol	**Gene_name**	**FBgn**	**Reference**	**DOI**
aly	always early	FBgn0004372	White-Cooper et al., 2000	https://doi.org/10.1242/dev.127.24.5463
aub	aubergine	FBgn0000146	Nishida et al., 2007	DOI: 10.1261/rna.744307
bam	bag of marbles	FBgn0000158	Schulz et al., 2004	DOI: 10.1534/genetics.103.023184
CadN	Cadherin-N	FBgn0015609	Boyle et al., 2007	DOI: 10.1016/j.stem.2007.08.002
can	cannonball	FBgn0011569	Hiller et al., 2001	DOI: 10.1101/gad.869101
cher	cheerio	FBgn0014141	Tanentzapf et al., 2007	DOI: 10.1038/ncb1660
CycB	Cyclin B	FBgn0000405	White-Cooper et al., 1998	DOI: 10.1242/dev.125.1.125
Dic61B	Dynein intermediate chain at 61B	FBgn0263988	Lu et al., 2020	DOI: 10.1101/gad.335331.119
dlg1	discs large 1	FBgn0001624	Papagianoulli and Mechler, 2009	DOI: 10.1038/cr.2009.71
esg	escargot	FBgn0287768	Kiger et al., 2000	10.1038/35037606
eya	eyes absent	FBgn0000320	Fabrizio et al., 2003	10.1016/s0012-1606(03)00127-1
f-cup	flyers-cup	FBgn0028487	Barreau et al., 2008	DOI: 10.1242/dev.021949
Fas3	Fasciclin III	FBgn0000636	Brower et al., 1981	https://doi.org/10.1242/dev.63.1.233
fzo	fuzzy onions	FBgn0011596	Hwa et al., 2002	DOI: 10.1016/s0925-4773(02)00141-7
hh	hedgehog	FBgn0004644	Michel et al., 2012	10.1242/dev.075242
Hml	Hemolectin	FBgn0029167	Li et al., 2022	DOI: 10.1126/science.abk2432
kl-2	male fertility factor kl2	FBgn0001313	Carvalho et al, 2000	10.1073/pnas.230438397
kl-3	male fertility factor kl3	FBgn0267432	Carvalho et al, 2001	10.1073/pnas.230438398
kl-3	male fertility factor kl3	FBgn0267432	Fingerhut et al., 2019	10.1371/journal.pgen.1008028
kl-5	male fertility factor kl5	FBgn0267433	Gepner and Hays, 1993	10.1073/pnas.90.23.11132
kl-5	male fertility factor kl5	FBgn0267433	Fingerhut et al., 2019	10.1371/journal.pgen.1008028
kmg	kumgang	FBgn0032473	Kim et al., 2017	DOI: 10.1126/science.aal3096
Mst77F	Male-specific transcript 77F	FBgn0086915	Barckmann et al., 2013	https://doi.org/10.1016/j.ydbio.2013.02.018
Mst84Db	Male-specific RNA 84Db	FBgn0004173	Kuhn et al., 1991	DOI: 10.1016/0925-4773(91)90064-d
Mst84Dc	Male-specific RNA 84Dc	FBgn0004174	Kuhn et al., 1991	DOI: 10.1016/0925-4773(91)90064-d
Mst87F	Male-specific RNA 87F	FBgn0002862	Kuhn et al., 1991	DOI: 10.1016/0925-4773(91)90064-d
MtnA	Metallothionein A	FBgn0002868	Zhao et al., 2010	doi: 10.1093/nar/gkp1006
Nep5	Neprilysin 5	FBgn0039478	Sitnik et al., 2014	DOI: 10.1534/genetics.113.160945
p53	p53	FBgn0039044	Monk et al., 2012	DOI: 10.1007/s00441-012-1479-4
p-cup	presidents-cup	FBgn0030840	Barreau et al., 2008	DOI: 10.1242/dev.021949
piwi	P-element induced wimpy testis	FBgn0004872	Gonzalez et al., 2015	DOI: 10.1016/j.celrep.2015.06.004
Rbp4	RNA-binding protein 4	FBgn0010258	Baker et al., 2015	https://doi.org/10.1242/dev.122341
sa	spermatocyte arrest	FBgn0002842	Hiller et al., 2004	DOI: 10.1242/dev.01314
shg	shotgun	FBgn0003391	Voog et al., 2008	DOI: 10.1038/nature07173
so	sine oculis	FBgn0003460	Fabrizio et al., 2003	DOI: 10.1016/s0012-1606(03)00127-1
soti	scotti	FBgn0038225	Barreau et al., 2008	DOI: 10.1242/dev.021949
stg	string	FBgn0003525	Alphey et al., 1992	https://doi.org/10.1016/0092-8674(92)90616-K
Syt1	synaptotagmin 1	FBgn0004242	Li et al., 2022	DOI: 10.1126/science.abk2432
tj	traffic jam	FBgn0000964	Li et al., 2003	DOI: 10.1038/ncb1058
tomboy20	tomboy20	FBgn0037828	Hwa et al., 2004	https://doi.org/10.1016/j.febslet.2004.07.025
upd1	unpaired 1	FBgn0004956	Tulina and Matunis 2001	DOI: 10.1126/science.1066700
vas	vasa	FBgn0283442	Hay et al., 1988	DOI: 10.1016/0092-8674(88)90216-4
wa-cup	walker cup	FBgn0037502	Barreau et al., 2008	DOI: 10.1242/dev.021949
zpg	zero population growth	FBgn0024177	Tazuke et al., 2002	DOI: 10.1242/dev.129.10.2529

the “saxophone” at the UMAP center, with early cyst cell nuclei extending down and leftward in a thin line. In addition, analysis by fluorescence *in situ* hybridization (FISH), and the average number of unique transcripts (Unique Molecular Identifier - UMI) expressed helped assign identity. For example, spermatocytes are highly transcriptionally active, whereas *Drosophila* early spermatids are nearly quiescent. While clustering was carried out using the Leiden algorithm at increasing levels of resolution, we settled on Leiden 6.0 as providing optimal granularity along both somatic and germline differentiation trajectories. We assigned 43 clusters as germline and 22 clusters as likely cyst cell lineage, with many inferred from the UMAP geography as representing putative intermediate cell types in the respective lineages (Figures 1F, 2A, 6A, and S1A).

Progression of differentiation in the male germ line stem cell lineage

Figure 2A shows the UMAP for the germ line stem cell lineage with Leiden 6.0 clusters labeled. Expression of the germ cell-specific gap junction gene *zero population growth* (*zpg),* required for survival of early spermatogonia (Tazuke et al., 2002) (Figure 2D, L), along with *vasa, stg* and *esg* (Figure 1C, D and E), further established nuclei at the pointed tip of the shark tail (clusters 25 and 22) as GSCs and spermatogonia. *In vivo*, GSCs are distinguished from gonialblasts and transit amplifying spermatogonia cytologically, by attachment to the apical hub and cell biological characteristics such as oriented centrosomes and spindles, and functionally, by lineage analysis. However, mRNA markers restricted to GSCs have not yet been identified, preventing us from determining what percent of these early nuclei are GSCs. Many nuclei in cluster 22 express *bag-of-marbles (bam)* (Figure 2L) but lack known spermatocyte markers, suggesting that these nuclei represent mid-to-late spermatogonia or germ cells undergoing premeiotic S phase. Moving rightward, several known early spermatocyte markers such as *kumgang* (*kmg)* and *RNA-binding protein 4* (*Rbp4*) began to be expressed (clusters 5, 78, and 40) (Figure 2F-G, L). Transcripts from *aubergine* (*aub),* a piRNA binding protein, were detected in the spermatogonial region (clusters 25, 22) and overlapping with early spermatocyte markers (clusters 5, 78, 40 and 41) (Figure 2E and L). Fluorescent *in situ* hybridization (FISH) confirmed *aub* transcripts present in GSCs around the hub, spermatogonia, and extending into early

Figure 2

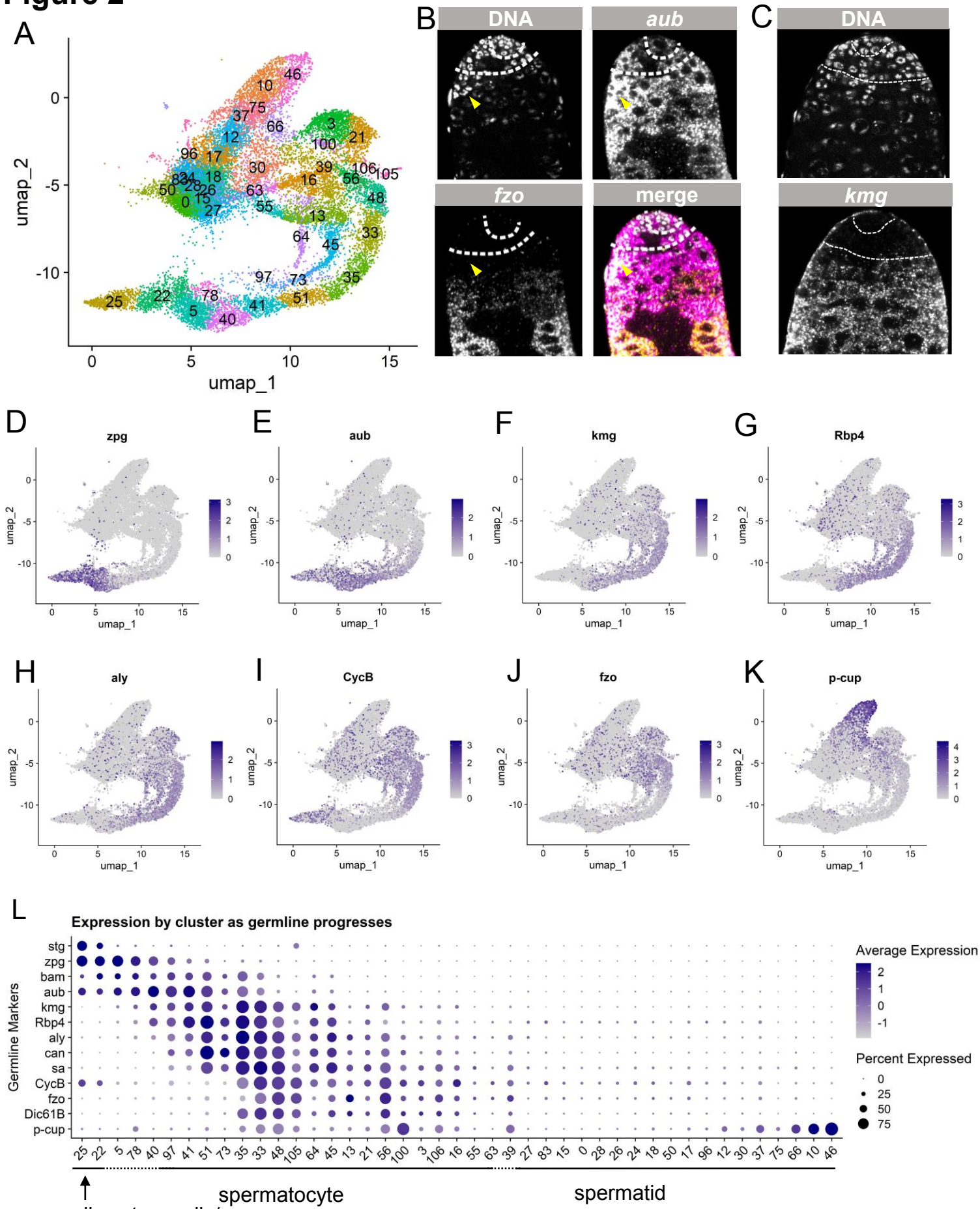

Figure 2 with one supplement

Characteristics of the germline lineage

A) Germline portion of the UMAP generated by Seurat from clustering of the full testis plus seminal vesicle dataset at Leiden 6.0 resolution. **B-C)** Apical tips of testes showing localized expression of **B)** *aub* (magenta) and *fzo* (yellow) mRNA and **C)** *kmg* mRNA visualized by *in situ* hybridization. Apical-most dotted line demarcates germ line stem cells (GSCs) around the hub from spermatogonia. Lower dotted line demarcates spermatogonia from young spermatocytes. Yellow arrowhead in **B**: early spermatocytes. **D-K)** Feature plots generated by Seurat showing expression levels of *zpg, aub, kmg, rbp4, aly, CycB, fzo,* and *p-cup* in the germline UMAP. Navy blue gradient bars: relative expression level for the indicated gene. **L)** Dot plot generated by Seurat showing expression levels of selected germline markers by cluster as nuclei progress from spermatogonia to spermatid. Color intensity: level of expression of the indicated gene averaged over all the nuclei in a given cluster relative to the level for that gene in other clusters. Size of dots: percent of nuclei in each cluster in which expression of the gene was detected. (see also FIgure 2 - figure supplement 1).

spermatocyte cysts, with their characteristic larger nuclei (Figure 2B). FISH also confirmed expression of *kmg* mRNA starting in early spermatocytes (Figure 2C), with early spermatocytes showing both *aub* and *kmg* transcripts, consistent with the snRNA-seq data.

Progressively maturing spermatocytes along the bottom right of the germline UMAP expressed later markers, including mRNAs for the spermatocyte-specific tMAC subunit *always early* (*aly)* and the testis-specific TAFs (tTAFs) *spermatocyte arrest (sa)* and *cannonball* (*can*) (clusters 41, 51, 35, and onward; Figure 2H,L). Expression of *fuzzy onions* (*fzo)* and *Dynein intermediate chain 61B* (*Dic61B*) was detected later, as the germ cell clusters curved upward (clusters 33, 48,105, 45, 13, 56; Figure 2J,L), consistent with the dependence of *fzo* and *Dic61B* transcription on *aly* (Hwa et al., 2002; Lu et al., 2020). Correlating *in vivo* morphology with gene expression space (visualized in the UMAP), *fzo* transcripts were not detected by FISH in the young spermatocytes near the spermatogonial region but were strongly detected in more mature spermatocytes further away from the testis apical tip (Figure 2B). The G2/M cell cycle regulator *CyclinB* (*CycB*) is transcribed from one promoter in mitotic spermatogonia, silenced, then re-expressed from an alternate promoter in later spermatocytes, dependent on *aly* function (Lu et al., 2020; White-Cooper et al., 1998). These two distinct stages of *CycB* transcript expression are clearly visible in the snRNA-seq data (Figure 2I,L). Maturing spermatocytes, marked by expression of Y-linked genes (Figure 3D), lie toward the top of the upward curve where the tail meets the torso of the shark. The progression of germ cell differentiation continues with early stage spermatids along the upper torso and head of the shark (marked by low UMI - see below). Mid-to-late elongation stage spermatids, marked by expression of *p-cup* mRNA, lie in the blunt projection toward the upper right of the UMAP (Figure 2K,L; clusters 66, 10, 46).

The order of clusters in expression space reflects differentiation in the lineage, as indicated by plotting the expression of known germline markers in each UMAP cluster (Figure 2L). Notably, using the published marker genes scored here, sequential cluster identities (e.g., 25, 22, 5, 78, 40) were not each delimited by unique marker genes. Instead, graded expression of the markers examined extended across boundaries between clusters. This was also observed in a UMAP with just nine clusters created at lower resolution (Figure S1B,C).

The geography of the UMAP is reminiscent of the spatio-temporal organization in the testis itself, with stages laid out from GSCs to transit amplifying spermatogonia, then young, mid, and late-stage spermatocytes. However, as the UMAP displays changes in gene expression rather than physical space, some surprisingly long stretches of the UMAP represent what are known to be relatively short periods in developmental time. For example, a large stretch along the bottom of the UMAP (clusters 5, 78, 40, 41, 51) represents young spermatocytes, previously thought of as a single, short developmental stage. This is underscored by the long gap in detection of *CycB* mRNA in these clusters (Figure 2I, L). In contrast, *in situ* hybridization showed only a relatively narrow region near the boundary between spermatogonia and spermatocytes devoid of *CycB* mRNA (White-Cooper et al., 1998). The territory of the UMAP containing clusters 5, 78, 40, 41, 97, 73, and 51 may be stretched out in gene expression space because the early spermatocyte stages are a time of extensive, rapid, and dynamic changes in gene expression: many genes are being dramatically upregulated as the spermatocyte expression program initiates, while a number of genes transcribed in spermatogonia are being downregulated (Figure 2B-H,L; Figure 3A; orange, tan and green cells in Figure 4A,C,F,G - see also Shi et al., 2020). Indeed, young spermatocytes are represented by fewer nuclei (2462; clusters 5, 78, 40, 41, 51) then more mature spermatocytes (~4100 nuclei; clusters 35, 33, 64, 45, 48, 105, 56, 13, 16). In addition, as early spermatocytes are still relatively small, they will occupy less physical space than more mature spermatocytes.

The spermatocyte transcription program

The spermatocyte period features onset of dramatic transcriptional changes. Many genes expressed in spermatocytes are transcribed in few or no other known cell types, including the markers *kmg, Rbp4, fzo, can, sa* (see references in Table 1). This robust onset of cell type-specific transcription appears as an increase in the number of different genes detected per nucleus (Figure 3A,C), leading to a substantial increase in transcriptome complexity. Coincident with this was a large increase in the number of unique molecular identifiers (UMI) scored, peaking in mid-to-late spermatocyte nuclei (clusters 35 and 33), with average UMI per cluster increasing from <5000 to >30,000 UMI per nucleus as spermatogonia differentiated to late spermatocytes

Figure 3

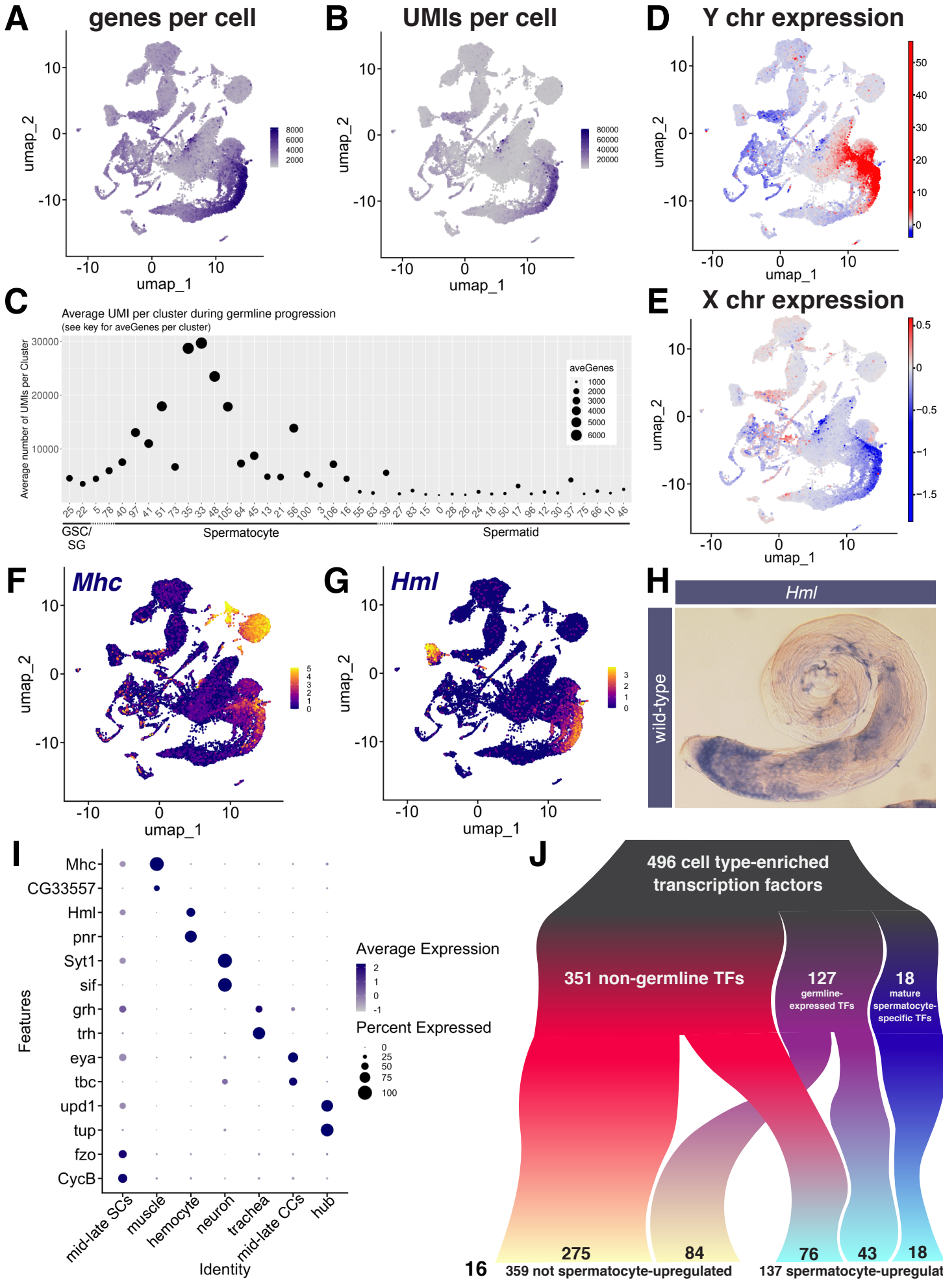

Figure 3 with one supplement

Features of the spermatocyte transcription program

(A,B) UMAPs of snRNA-seq data showing: **A)** number of genes detected as expressed and **B)** number of unique molecular identifiers (UMIs) detected per nucleus. **(C)** Plot of average number of genes expressed (dot size) and UMIs detected per nucleus per germline-annotated Leiden 6.0 cluster, ordered by progression of germ line differentiation. **(D,E)** UMAPs of snRNA-seq data showing the average expression of: **D)** transcripts on the Y chromosome or **E)** transcripts on the X chromosome relative to an expression-matched control set (gene sets with binned expression matching transcript lists). (Note the dramatically different scales in D vs E.) UMAPs taken directly from ASAP (Li *et al.*, 2022, Gardeux *et al.*, 2017). **(F,G)** UMAP plots of snRNA-seq raw counts (log-transformed) showing expression of: **F)** *Myosin heavy chain* (*Mhc*) in muscle and late spermatocytes and **G)** *Hemolectin* (*Hml*) in hemocytes and late spermatocytes. Yellow: relative expression high. **H)** Testis hybridized *in situ* with biotinylated antisense RNA probe to *Hml,* showing expression (blue) in spermatocytes. **I)** Dot Plot showing expression of pairs of tissue-specific markers across cell types. Average expression of each gene in a given cell type denoted by color intensity. Percent of cells of the given cell type that express each gene denoted by dot size. **J)** Flow chart showing whether 496 predicted transcription factors identified as relatively cell type specific in the FCA study (Li *et al.*, 2022) (top of chart) were detected as upregulated in spermatocytes in our analysis of testis plus seminal vesicle snRNA-seq (bottom of chart; see Figure 3 - source data 1, and Methods). (see also FIgure 3 - figure supplement 1).

(Figure 3B,C). The FCA paper noted that testis, heart, fat body, Malpighian tubules, and male reproductive glands had relatively high RNA levels and number of genes expressed compared to other tissues (Li et al., 2022). Reanalysis showed that mid-to-late spermatocyte nuclei exhibited the highest complexity of all, with average expressed gene (6,000 compared to 2,000) and UMI (30,000 compared to <20,000) numbers higher than for any cluster mapped in heart, Malpighian tubules, or male reproductive glands (Figure 3 - figure supplement 1A; the high fat body signal was due to contaminating spermatocytes). High transcriptome complexity has also been noted in mammalian spermatocytes (Soumillon et al., 2013).

After peaking in clusters 35 and 33, UMI values per nucleus decreased through clusters 48, 105, 56, 106, 21, where the “tail” meets the “torso” of the shark, consistent with the observed lower expression of spermatocyte marker genes (Figure 2L). In the shark upper torso and head, many clusters had very low UMI (Figure 3C), making developmental order difficult to assign. This is reflected in the UMAP shape, with clusters grouped rather than extended along a string as in early germ cell stages. We surmise these nuclei represent early spermatids, as classic studies showed that transcription falls dramatically from shortly before onset of the meiotic divisions, with no bulk incorporation of radioactive uridine detected in haploid round and early elongating spermatid nuclei (Gould-Somero and Holland, 1974; Olivieri and Olivieri, 1965).

Spermatocytes showed sex chromosome specific trends in gene expression changes. Overall, Y-linked transcripts were strongly upregulated in spermatocytes (Figure 3D), primarily driven by the robust expression of 8 of the 12 single copy genes. For example, transcription of the Y-linked fertility factors *kl-3* and *kl-5*, which encode flagellar dyneins expressed only in male germ cells, was massively upregulated (125 and 275 fold, respectively with similarly large differences in absolute expression). As 10X sequencing utilizes oligo(dT) primers, the late appearance of reads from the Y-linked fertility factors in spermatocytes may reflect the very long time required to complete synthesis of the mature transcripts, which have extremely large introns (Fingerhut et al., 2019). For X linked genes, analysis of the snRNA-seq data showed a similar level of expression relative to a control set of genes from all chromosomes in spermatogonia and early spermatocytes. However mid-to-late spermatocytes featured a transition to reduced

expression of X-linked genes relative to the control set (Figure 3E), consistent with the roughly 2 fold lower expression of X linked genes compared to generally expressed autosomal genes observed previously (Mahadevaraju et al., 2021).

One surprise that emerged from the UMAP geography was that later stage spermatocytes split into three parallel streams, all expressing spermatocyte specific markers. (Figure 2A). Strikingly, nuclei in the leftmost and middle streams (clusters 64 and 45, respectively) had considerably lower UMI count than in the robust mainstream (cluster 35; Figure 3B,C). The cause underlying such different UMI levels among late spermatocytes is not known, but could suggest a stochastic component to meiotic chromosome condensation and the attendant chromosome-wide downregulation in gene expression.

A second notable feature was the expression in mid-to-late spermatocytes of many markers classically associated with other cell types. Notably, markers for muscle *(Myosin heavy chain* - *Mhc*), hemocytes (*Hemolectin* - *Hml,*) neurons (*Synaptotagmin* - *Syt1*), and epithelial cells (*grainy head* - *grh*) selected as identifiers of these cell types in the FCA study of adult *Drosophila* tissues (Li et al., 2022), were upregulated in late spermatocytes (Figure 3F,G,I). This was confirmed by in situ for Hml (Figure 3H - figure supplement 1D,E,H). Several mRNAs normally thought of as markers of somatic cells, *eyes absent* (*eya*) and *unpaired 1* (*upd*) for example, were detected as upregulated in mid-to-late spermatocytes (Figure 3 - figure supplement 1F,G). Expression of the RNAs was usually lower in spermatocytes than in the “marker” tissue, and not all genes characteristically expressed in marker tissue were detected as expressed in spermatocytes (Figure 3I, see also *tj* (Figure 1B) compared to *eya* (Figure 3 - figure supplement 1F). Similar upregulation of *Mhc*, *Hml*, *grh,* and *Syt1* in spermatocytes was independently observed in a single cell testis dataset to be introduced below (Figure 3 - figure supplement 1I), so is not likely to be an artifact of isolation of nuclei. The cause of this seemingly promiscuous expression of certain genes, whether the encoded proteins accumulate, and what role, if any, these genes may have in the biology of spermatocytes remain to be investigated.

Although spermatocytes feature an overall increase in UMIs per cell, not all genes are promiscuously upregulated in spermatocytes. For example, across all adult fly tissues, the FCA

project identified 496 transcription factors predicted to have a high tissue specificity score (Li et al., 2022). That analysis predicted 351 of these as expressed in certain somatic cell types but not in germ line (Figure 3J, top). Our analysis of the testis plus seminal vesicle portion of the FCA data showed that only about a fifth (76) of these 'somatic' factors were upregulated in spermatocytes compared to spermatogonia, with most (275) exhibiting no upregulation (Figure 3J bottom; Figure 3 - source data 1). This again suggests that there is some specificity to the 'promiscuous expression' in spermatocytes.

sn vs. scRNA-seq: dynamics of active transcription vs. stored RNAs

Although largely transcriptionally silent, early spermatids carry numerous cytoplasmic transcripts, many of which are recruited to be translated for temporal control of protein expression during spermatid morphogenesis (Schäfer et al., 1990, 1995). As single-nucleus sequencing detects recently transcribed or nuclear resident transcripts, comparison of snRNA-seq with *single cell* RNA-seq (scRNA-seq) data should identify genes no longer actively transcribed at a particular stage but represented by mRNAs retained/perduring from earlier transcription. Single cell RNA-seq of testes yielded data for 6438 germ cells after quality control steps (Materials and Methods). Indeed, comparison of snRNA-seq and scRNA-seq allowed mapping of dynamic changes in transcriptional activity alongside identification of an extensive array of post-transcriptionally retained (perduring) transcripts stored for later use.

The UMAP geography for both the snRNA-seq and scRNA-seq datasets showed progression from spermatogonia to spermatids, with germline differentiation classes present in sequential order (Figure 4A-D). In the scRNA-seq UMAP, as for snRNA-seq, expression of *zpg* marked a small number of spermatogonia located at the bottom tip, *aub* marked those same plus additional cells, presumably early spermatocytes, *fzo* marked differentiating spermatocytes, and *presidents-cup* (*p-cup*) marked later elongating spermatids in an arm extending from the top of the UMAP (Figure 4E). Corroborating these expression patterns, FISH to whole mount testes clearly showed *aub* expression in spermatogonia and early spermatocytes, and *fzo* expression beginning in spermatocytes (Figure 4F). Notably, *fzo* mRNA was abruptly downregulated in early round spermatids soon after the second meiotic division (Figure 4F, arrowhead).

Figure 4.

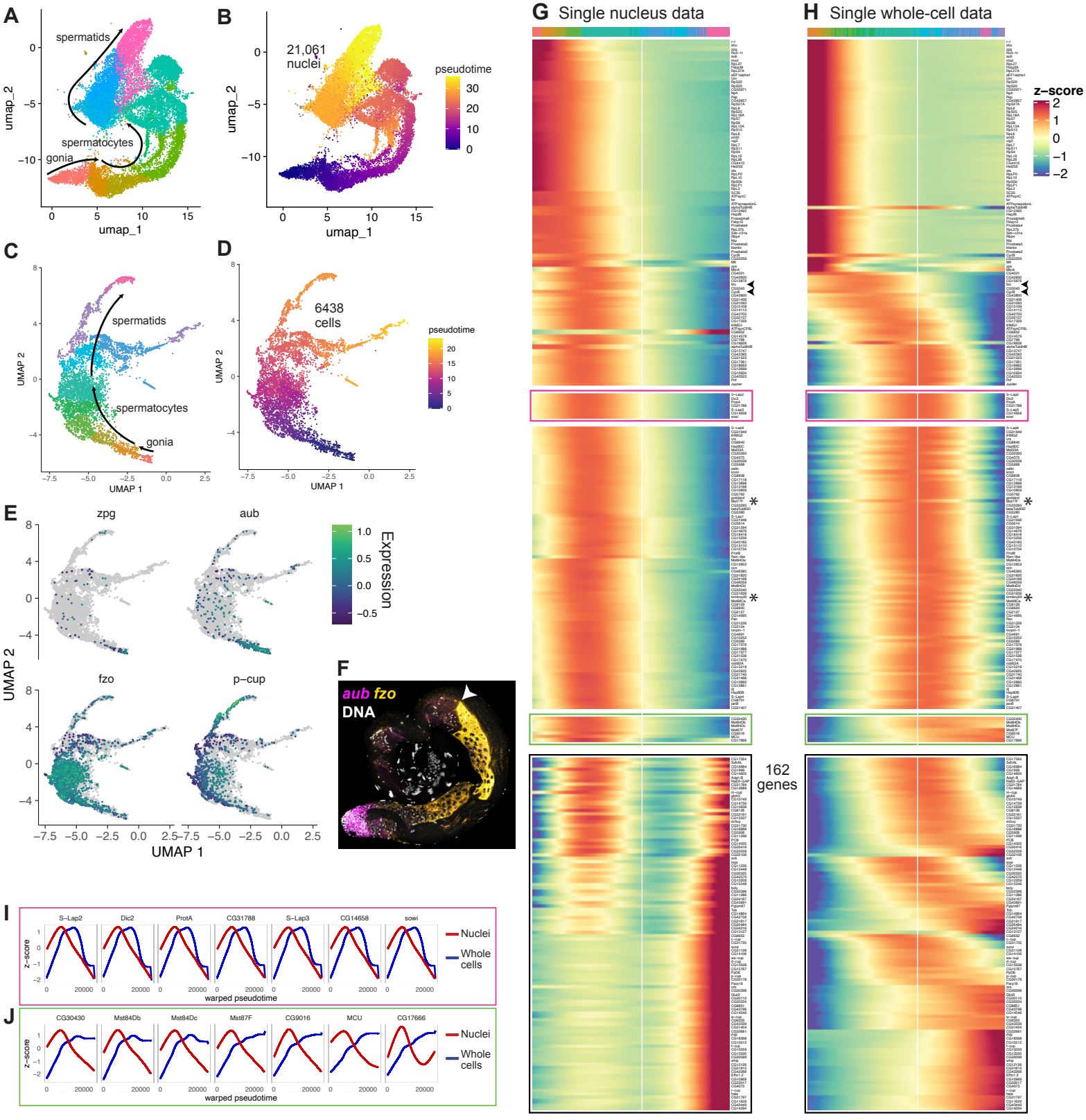

Figure 4

Developmental transitions revealed by comparing sn and scRNA-seq

(A-D) UMAP plots of germline-annotated data from **A,B)** FCA snRNA-seq of adult testis plus seminal vesicle and **C,D)** whole-cell scRNA-seq of adult testis. **A,C)** Color denotes germline differentiation stage. **B,D)** Color denotes pseudotime, with the few nuclei lacking a calculable pseudotime value colored gray. **E)** UMAPs of scRNA-seq data showing log10(Expression) levels of cell-stage diagnostic markers *zpg*, *aub*, *fzo*, and *p-cup*. **F)** FISH of diagnostic genes *aub* and *fzo*. Arrowhead marks end of *fzo* expression in early round spermatids. **(G-H)** Heatmaps of row-normalized (z-score) gene expression over pseudotime for: **G)** all germline-annotated single nuclei from panel A, **H)** all germline-annotated single whole cells from panel C, with genes in same order as in G. X axes, pseudotime; Y axes, genes. Vertical white line: nuclei (G) or cells (H) where level of fzo mRNA has dropped half way (0 on Z score). Top bars: cell identity for each column, colored as in panels A,C. Black boxes: genes transcribed post-meiotically (see Figure 5). **(I-J)** Comparison of gene expression over warped pseudotime for: **I)** genes outlined by pink boxes in G,H; **J)** genes outlined by green boxes in G,H.

Trajectory inference can assign a differentiation distance parameter to cells inferred from transcriptional differences, with distance noted as 'pseudotime' (Trapnell et al., 2014). Applying trajectory inference independently to the snRNA-seq and scRNA-seq germ line datasets produced contiguous trajectories. Using Monocle3, 99.9% (21,061/21,091) of the snRNA-seq germline nuclei were connected (Figure 4B). Notably, unlike prior trajectory analysis using Slingshot (Li et al., 2022), the inferred trajectory was contiguous, connecting cells of all differentiation points from early spermatogonia to late spermatids. Likewise, Monocle3 analysis of the 6438 germline cells from the scRNA-seq also produced a contiguous trajectory from spermatogonia to elongating spermatids, although it did include a late bifurcation, the explanation of which may be technical or biological. For both datasets, pseudotime staging paralleled the ordered trajectory deduced from marker gene expression in UMAP clusters. (Figure 2, Figure 4A-E).

Plotting normalized gene expression across pseudotime in the sn- and scRNA-seq datasets revealed both shared and contrasting dynamics. In both datasets, the same set of genes were expressed in early germ cells, with expression diminishing over pseudotime (Fig 4G,H; red/orange in the top color bar, corresponding to colors in Figure 4A,C). Similarly, some genes, including *fzo* and *CycB* (arrowheads) reached their peak expression in spermatocytes and dropped to low levels by early spermatid stages in the scRNA-seq (see vertical white line, Figure 4G,H), consistent with published *in situ* hybridization data (White-Cooper et al., 1998 and Figure 4F).

Interestingly, in the snRNA-seq dataset, a group of over 200 genes in the middle region of the heat map reached peak expression in the mid-spermatocyte stages (green-aqua hues in the top color bar) then dropped in expression, falling halfway to their nadir at a point similar to the drop in *fzo* and *cycB* expression (vertical white line) (Figure 4G). In the scRNA-seq dataset, however, these same genes were still at or near peak mRNA accumulation (red) in the same cells in which expression of *fzo* and *cycB* had already dropped (Figure 4H). Thus it is the comparison of the datasets that is most revealing: these genes are transcribed in spermatocytes, then transcription halts (inferred from the snRNA-seq dataset), but their mRNAs remain high in

spermatids (inferred from the scRNA-seq dataset) well past the stage when *fzo* and *cycB* mRNAs disappear (inferred from both datasets). Several genes from this set, including *Male-specific transcript 77F* (*Mst77F*) and *tomboy20* (asterisks), have been previously demonstrated by *in situ* hybridization to maintain abundant transcripts in both spermatocytes and elongating spermatids (Barckmann et al., 2013; Hwa et al., 2004). Comparison of the snRNA-seq and scRNA-seq datasets suggests that such a pattern, previously described for a small number of transcripts, is shared by hundreds of genes.

Comparison of single cell and single nucleus data revealed several distinct classes of transcript behaviors in spermatids, each worthy of targeted follow-up study. Notably, perduring transcripts from the class of genes described above showed two types of behavior. For most genes, transcripts disappeared sharply in later elongating spermatids (examples in pink box in Figure 4G,H). To plot transcript levels in the sn- and scRNA-seq datasets on the same X axes, a common 'warped' time scale was derived for the datasets (see Materials and Methods). First, for all genes upregulated in spermatocytes, onset of transcription in the nuclear transcriptome was followed (with delay) by upregulation in the whole-cell transcriptome, generally dominated by cytoplasmic transcripts (Figure 4I,J). As seen in the heat map (Figure 4H), the graphs for the pink box genes show that the mRNAs remained at peak levels considerably later in the scRNA-seq than in the snRNA-seq data, but the transcripts were eventually strongly downregulated by late spermatid stages (Figure 4I: blue lines). This suggests complexity in mRNA regulation in the cytoplasm: stable maintenance in early spermatids and abrupt degradation in later spermatids, perhaps once transcripts have been translated. Interestingly, the protein products of several of these genes are present and functional in late spermatids and sperm (Raja and Renkawitz-Pohl, 2006), suggesting these proteins are actively maintained in the absence of new translation.

A second type of behavior was noted for a small group of genes (green box in Figure 4G,H, graphed in J) where transcripts perdured even longer, remaining high through the latest stages assessed by scRNA-seq (blue lines in Figure 4J). As differentiation of late spermatocytes to late spermatids takes days (Chandley and Bateman, 1962), these remarkable transcripts maintained high levels of cytoplasmic abundance, with almost no sign of degradation, even days

after active transcription had dropped off. This suggests exceptional stability, likely provided by specialized RNA-binding proteins. Some such transcripts, encoded by *Mst84Db*, *Mst84Dc*, and *Mst87F*, have long been recognized to be translationally regulated, with perdurance in the cytoplasm for up to three days (Kuhn et al., 1991; White-Cooper et al., 1998). Others, including *CG30430, CG9016, MCU*, and *CG17666* have not been previously reported to undergo translational regulation. The differences in degradation timing revealed by scRNA-seq (Figure 4G-J, pink vs green boxes) may hint that distinct groups of RNAs, and thus their protein products, are engaged at different stages of spermatid morphogenesis.

Another compelling example of the utility of comparing snRNA-seq and scRNA-seq data is highlighted by the group of genes outlined in black (Figure 4G,H). In the snRNA-seq dataset, these genes are expressed in spermatocytes but transcription shuts down in early spermatids and remains off for a considerable period before expression is activated again in mid-to late elongation stages. Thus, few transcripts bridge the gap between late spermatocytes and mid-stage elongating spermatids, as if the two stages were disconnected. In contrast, in the scRNA-seq dataset, many of these same genes showed continued high transcript levels throughout the spermatid stages, presumably representing storage of mRNAs in the cytoplasm (Figure 4G,H, black boxes). In consequence, the mature spermatocyte to elongating spermatid stage transcriptomes were well connected through a smooth gradient of transcript levels in scRNA-seq data.

Reactivation of transcription in mid-to-late elongating spermatids

The ability of snRNA-seq to highlight dynamic transcriptional changes during cellular differentiation revealed striking transcriptional (re)activation of a subset of 162 genes in mid-to-late elongating spermatids, a phenomenon previously described for only 24 genes, "called post-meiotic transcripts" (Barreau et al., 2008). UMI counts and average number of genes expressed in the snRNA-seq were relatively low in post-meiotic clusters compared to other germ cell clusters (Figure 3C), consistent with the long-held idea that spermatids are nearly transcriptionally silent. Nonetheless, post-meiotic transcription appeared more extensive than previously appreciated, with transcripts from approximately 1000 genes detected. Analysis for genes specifically

Figure 5

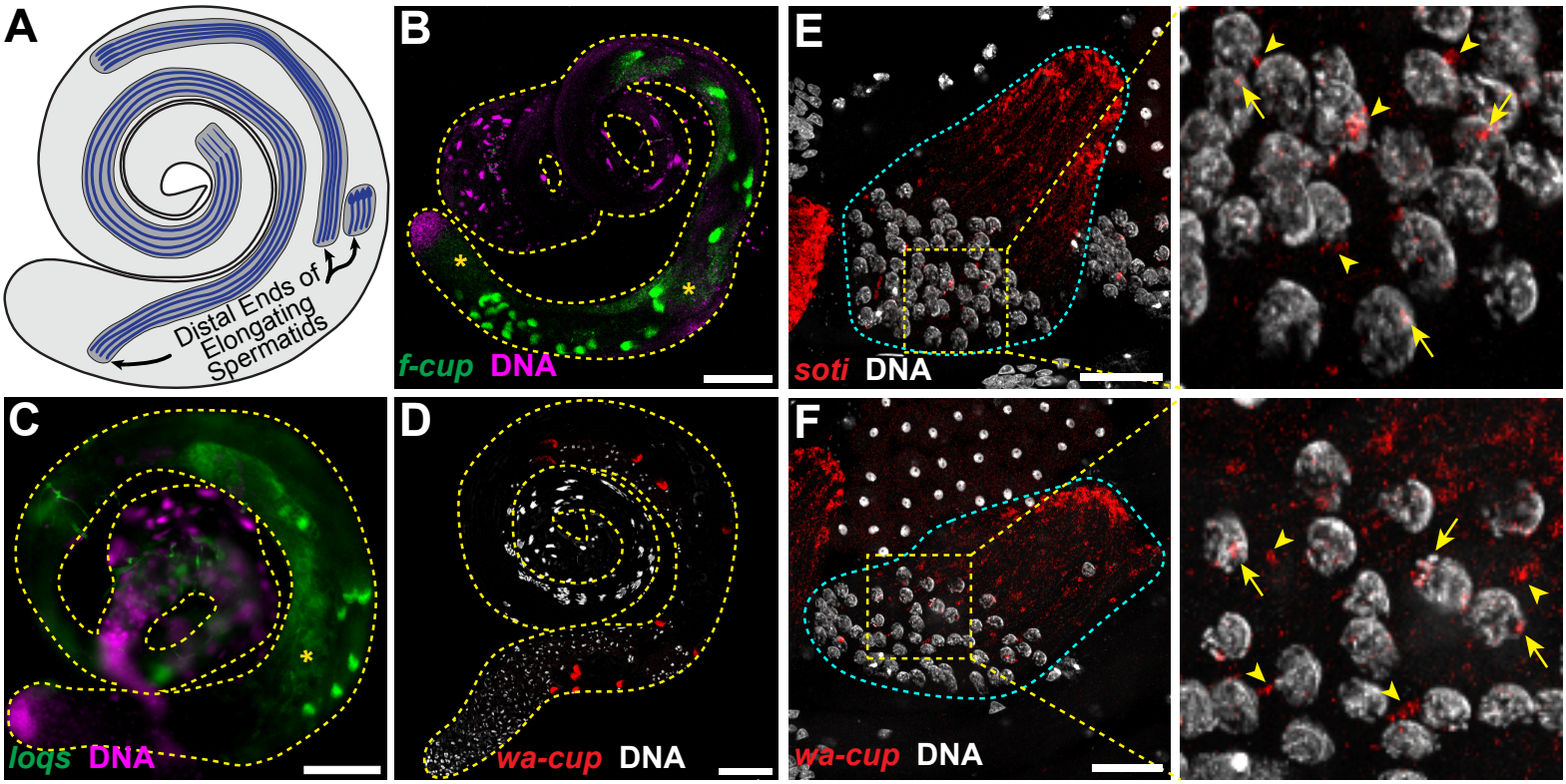

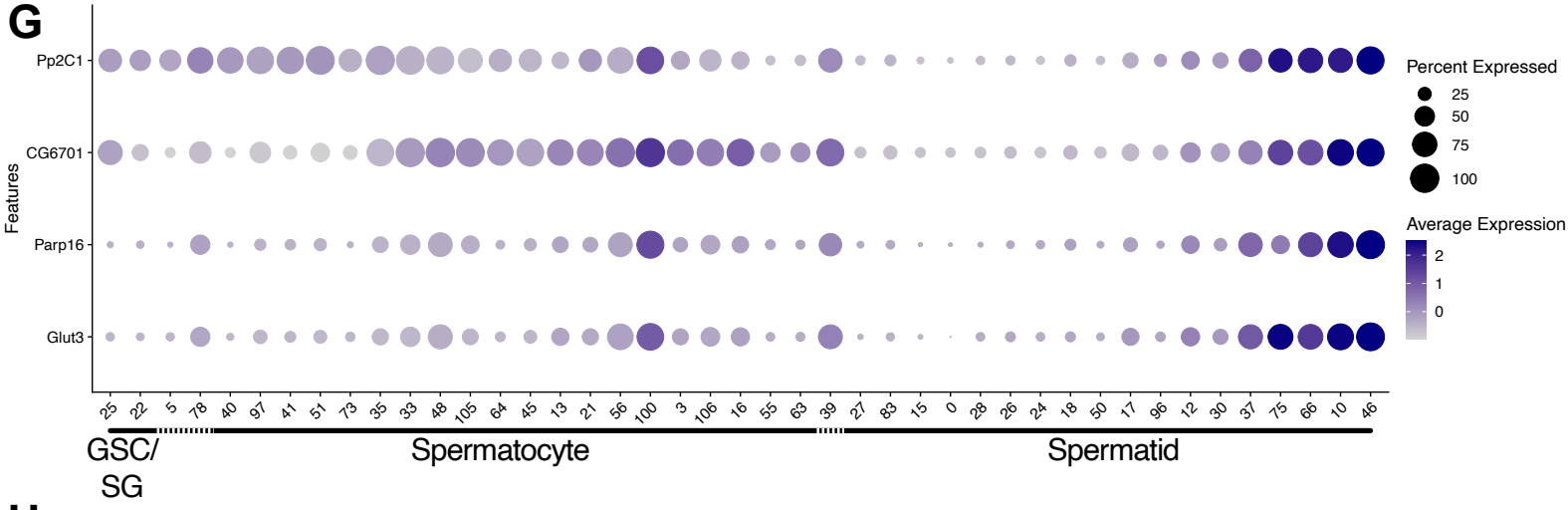

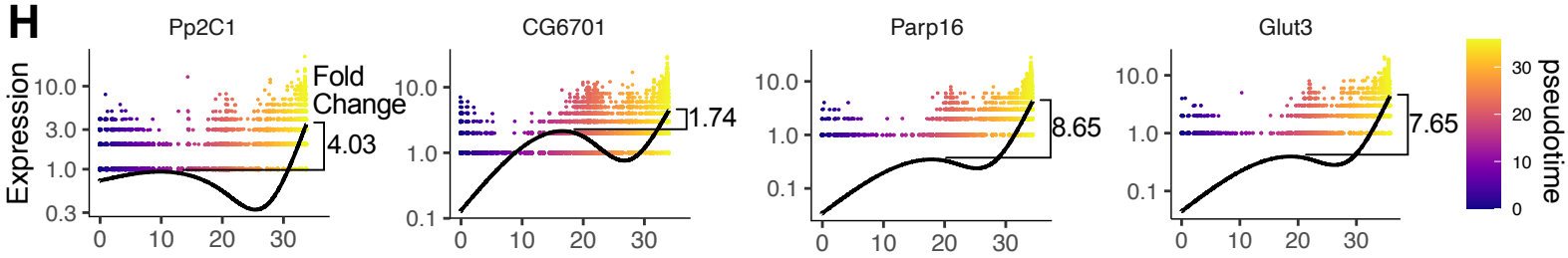

Figure 5 with one supplement

The transcript landscape of haploid spermatids

A) Diagram of spermatid orientation in the testis at different stages of spermatid elongation. Arrows: distal ends of spermatid cysts. (**B,C)** RNA FISH of representative transcripts (**B**: *f-cup*, **C**: *loqs*) in whole testes showing different patterns of mRNA localization for post-meiotically transcribed genes. DNA (magenta), target RNA (green). Asterisk: signal in spermatocytes. Bar: 100µm. **D)** smFISH for *wa-cup* (red) in whole testes. DNA (white). Bar: 100µm. (**E,F)** Left: smFISH for *soti* **E**) or wa-cup **F**) in a single early elongating spermatid cyst (cyan dashed line). RNA (red) and DNA (white). Bar: 25µm. Right: Enlarged image of yellow dashed box showing spermatid nuclei. Arrows: nuclear transcripts. Arrowheads: perinuclear granules. **G)** Dot plot for selected spermatid transcribed genes showing expression levels in each germ cell cluster. **H**) Expression over pseudotime for selected spermatid transcribed genes and fold change between late pseudotime and previous expression maxima in early/mid pseudotime. (see also FIgure 5 - figure supplement 1).

enriched in late pseudotime identified a list of 162, here termed spermatid transcribed genes (Figure 4G, black box, and Figure 5 - source data 1). These included 18 of the previously identified 24. FISH revealed *flyers-cup* (*f-cup*) RNA at the distal end of elongated spermatid bundles, as expected (Barreau et al., 2008, Figure 5A,B; Figure 5 - figure supplement 1A). RNA from *loquacious (loqs)*, a newly identified spermatid transcribed gene, was similarly localized (Figure 5C; Figure 5 - figure supplement 1B). Transcripts from *walker cup* (*wa-cup*) and *scotti* (*soti*) also localized to the distal ends of elongating spermatids as expected (Barreau et al., 2008, Figure 5D-F; Figure 5 - figure supplement 1C, D). Analysis of earlier elongating spermatid cysts by single molecule RNA FISH (smFISH) supports active transcription of *wa-cup* and *soti* in spermatids: smFISH revealed foci in spermatid nuclei, suggesting nascent, post-meiotic transcription (Figure 5E,F, arrows), as well as perinuclear granules (arrowheads), which could represent newly synthesized RNAs being trafficked toward the distal ends of the spermatids.

Analysis of the snRNA-seq data showed that many newly identified spermatid transcribed genes, including *Pp2C1* and *CG6701*, were initially expressed in spermatocytes or spermatogonia, downregulated in early spermatids, and later reactivated during mid-to-late elongation (Figure 4F-upper half of black box; Figure 5G,H). Other newly identified spermatid transcribed genes, including *Parp16* and *Glut3,* were weakly expressed in spermatocytes but robustly transcribed in elongating spermatids (Figure 4F - lower half of black box; Figure 5G,H). Both patterns are consistent with RT-qPCR and RNA *in situ* hybridisation results for the 24 post-meiotic transcripts previously identified (Barreau et al., 2008). Together the results show two sources of RNAs in elongating spermatids: cytoplasmic perdurance of RNAs transcribed in spermatocytes (Figure 4H), and *de novo* post-meiotic (re)activation of transcription of certain genes (Figure 4G, Figure 5G,H).

The majority of the spermatid transcribed genes remain functionally uncharacterized, and await investigation. GO term analysis showed no significant enrichment for any single biological process or pathway, although several functional classes were represented (Figure 5 - source data 1). Additionally, genes in this set did not appear to be coordinately reactivated, as by a single regulatory circuit. Rather, the likelihood of genes to be (re)activated concordantly was weakly correlated with their expression level, with a few outliers (Figure 5 - figure supplement 1E).

Progression of differentiation in the somatic cyst cell lineage

Somatic cyst cells govern many germline transitions, from stem cell behavior through sperm maturation and release (Figure 1A, 6O). The snRNA-seq approach may be especially useful for characterizing cyst cell transcriptomes across differentiation stages because the long, thin, extended shape of many cyst cell types may make isolation of intact cells difficult.

Cyst lineage identity was assigned by expression of three transcriptional regulators, *traffic jam* (*tj*), *eya* and *sine oculis* (*so*) (Figure 1B; Figure 6A,B,V; Figure 6 - figure supplement 1C,D). While both very early clusters (62, 36, 58) and very late clusters (72, 79, 84) were simple to describe (see below), the middle region of the 2-D UMAP presented a tangle. However, re-projecting the lineage to preserve a third dimension clarified the assignment of cluster order through the middle region (Figure 6C; Materials and Methods for a rotatable 3-D version). This, combined with pseudotemporal ordering (Figure 6 - figure supplement 1A,B) and marker analysis, enabled us to assign specific cyst cell clusters to stem cell, spermatogonial, spermatocyte, spermatid or sperm release stages of germline development. The few clusters difficult to assign, perhaps notably, had relatively low UMI count (FIgure 6E).

The cyst lineage begins with proliferative *stg*-expressing CySCs (Cluster 62, Figure 1D; Figure 6A,D). Expression of *tj* suggested that clusters 36 and 58 represent early-stage cyst cells that enclose transit amplifying spermatogonia (Figure 6B,V) labeled SgCC in Figure 6D, as Tj protein marks the nucleus of these early cyst cells but is not detected by immunofluorescence staining in spermatocyte-associated cyst cells (Li et al., 2003; Zoller and Schulz, 2012). Complementing this, *CG3902* was also detected in the same nuclei as *tj*, and a CG3902 protein trap line revealed cytoplasmic protein accumulation up to early ScCC and no detectable protein thereafter (Figure 6V; Figure 6 - figure supplement 1E,F). *P-element induced wimpy testis* (*piwi*) mRNA was enriched in the same clusters as *tj and CG3902*, and also was detected at lower levels in nuclei of subsequent clusters (for example, clusters 47 and 77; Figure 6D SgCC and ScCC, F,V) (Gonzalez et al., 2015). FISH and analysis of a Piwi protein trap confirmed expression in early cyst cells associated with spermatogonia at the testis apex, as well as in cyst cells enclosing

Figure 6

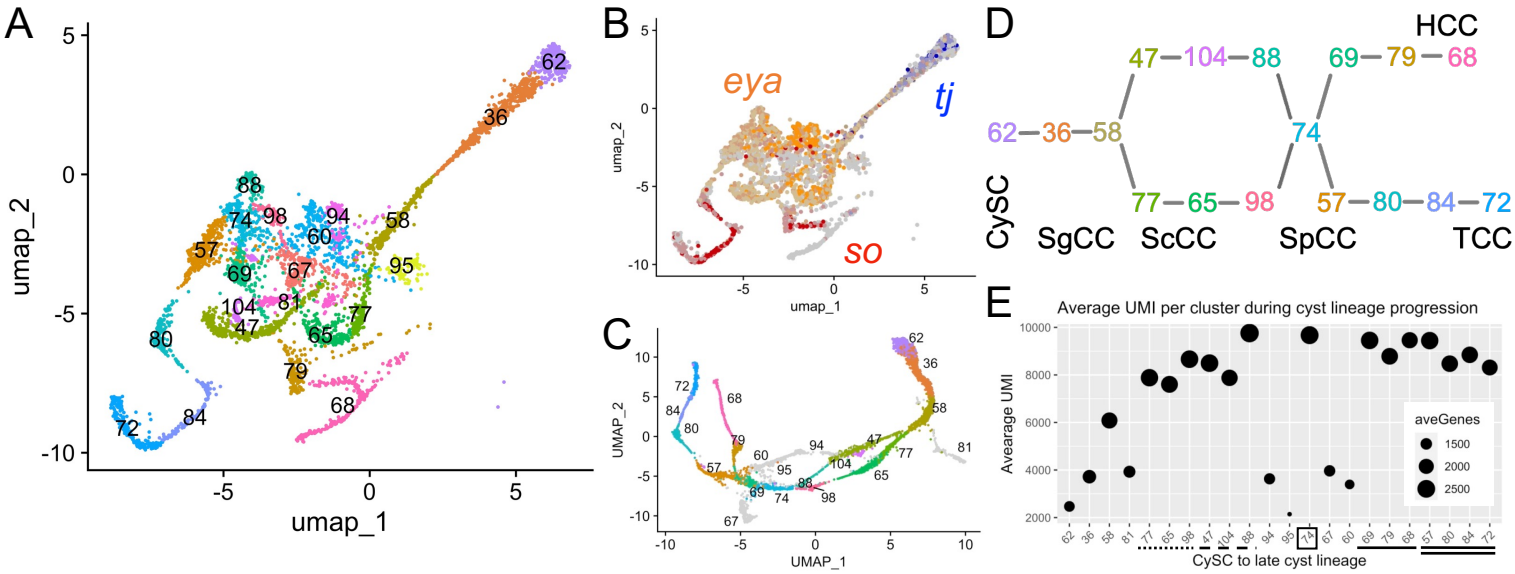
A
umap_2
umap_1
B
eya
tj
so
umap_2
umap_1
C
UMAP_2
UMAP_1
D
HCC
CySC
SgCC
ScCC
SpCC
TCC
E
Average UMI per cluster during cyst lineage progression
Avearage UMI
aveGenes
1500
2000
2500
CySC to late cyst lineage

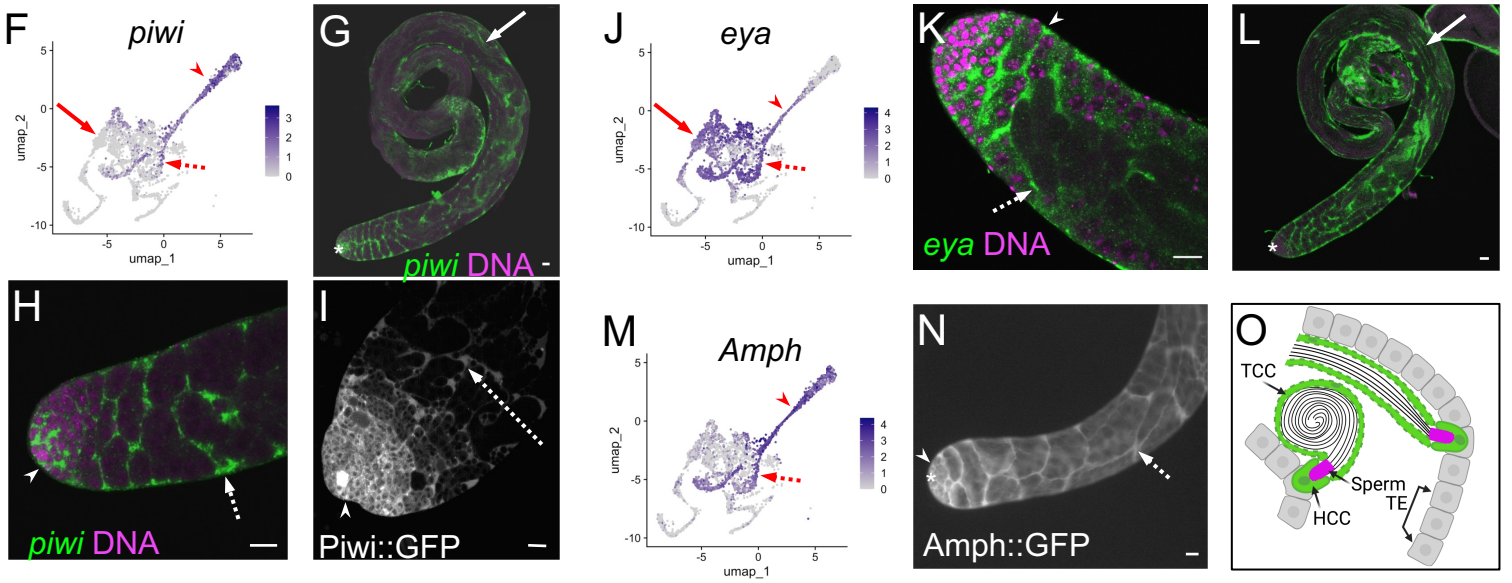
F
piwi
G
piwi DNA
H
piwi DNA
I
Piwi::GFP
J
eya
K
eya DNA
L
M
Amph
N
Amph::GFP
O
TCC
Sperm
TE
HCC

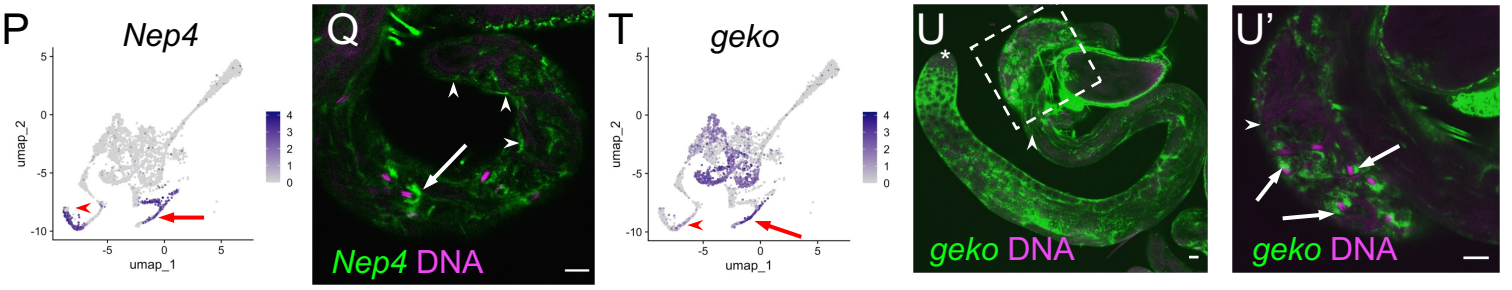
P
Nep4
Q
Nep4 DNA
T
geko
U
geko DNA
U'
geko DNA

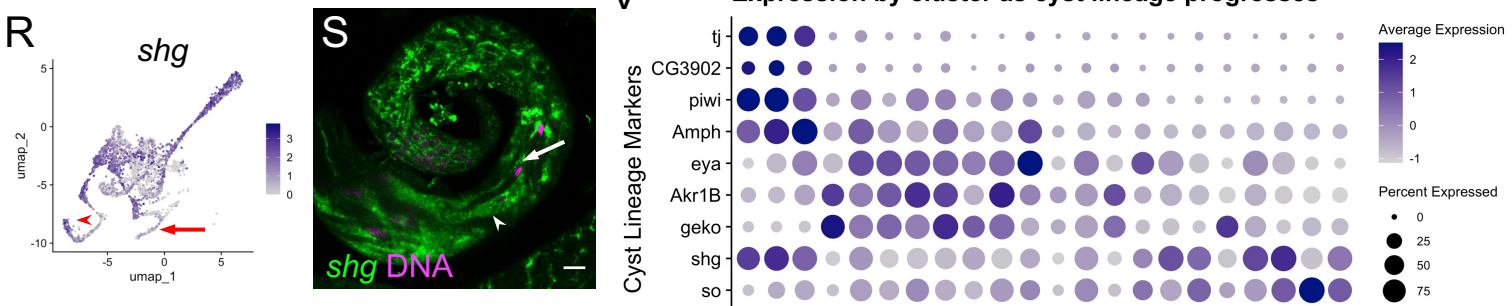
R
shg
S
shg DNA
V
Expression by cluster as cyst lineage progresses
Cyst Lineage Markers
tj
CG3902
piwi
Amph
eya
Akr1B
geko
shg
so
Nep4
Average Expression
Percent Expressed
CySC to late cyst lineage

Figure 6 with one supplement

Differentiation in the somatic cyst cell lineage

A) Cyst cell lineage portion of the UMAP from snRNA-seq data with Leiden 6.0 cluster numbering. **B)** Expression of *tj* (blue), *eya* (orange), and *so* (red) projected on the UMAP (heatmaps in FIgure 6 - figure supplement 1C,D). **C)** 2D UMAP of cyst cell clusters newly reprojected in their own gene expression space (Materials & Methods; note different axis coordinates relative to panel A). Cluster colors correspond to panel A except for unidentifiable clusters with low UMIs (gray). **D)** Schematic of cyst cell cluster progression from CySC, to spermatogonia-associated (SgCC) to spermatocyte-associated (ScCC) to Spermatid-associated (SpCC) inferred from the 3D UMAP in panel C. Cluster numbers and colors as in A. Note two splits, one earlier and one later in cyst lineage progression. **E)** Plot of average number of genes (dot size) and average number of UMIs per cyst lineage-annotated cluster; with clusters ordered by progression of differentiation. Dotted and dashed lines under cluster numbers represent the early split shown in D, while single (HCC) and double (TCC) solid lines represent the later split. **F - U)** In these panels, a UMAP is compared to a set of FISH and/ or IF images. For each gene comparison, arrows, dashed arrows and/or arrowheads point out the same cell type in the UMAP and its corresponding FISH and/ or IF image. **F)** *piwi* mRNA expression projected on the UMAP. **(G,H)** *piwi* mRNA (FISH; green) and DNA (magenta). **G**) whole testis, and **H)** testis tip view. **I)** Apical tip of testis expressing GFP protein trap of Piwi. **J)** *eya* mRNA expression projected on the UMAP. **(K, L)** *eya* mRNA (FISH; green) and DNA (magenta), **K**) Testis apical tip. **L)** Whole testis. **M)** *Amph* expression projected on the UMAP. **N)** Testis apical third expressing GFP protein trap of Amph**. O)** Schematic of the head cyst cell (HCC, green solid outline) embedded in the terminal epithelium (TE, gray), with the tail cyst cell (TCC, green dashed outline) extending away, containing either a pre-coiled (top) or coiled (bottom) spermatid bundle (nuclei, magenta). **P)** *Nep4* mRNA expression projected on the UMAP. **Q)** Testis base showing *Nep4* mRNA (FISH, green) and DNA (magenta). **R)** *shg* mRNA expression projected on the UMAP. **S)** Testis base showing *shg* mRNA (FISH, green) and DNA (magenta). **T)** UMAP of *geko* mRNA expression. **U)** Whole testis showing *geko* mRNA (FISH, green) and DNA (magenta). **U')** Inset outlined by white dashed box in U showing base of testis. **V)** Dotplot of gene expression (Y axis) by cluster as cyst lineage progresses through differentiation (X axis, left to right). Degree of expression in each cluster indicated by color scale. Percent of

cells within a cluster expressing the gene indicated by size of dot. Lines under cluster numbers as in E. Asterisk denotes hub. Bars: 20μm. (see also Figure 6 - figure supplement 1).

growing spermatocyte cysts (Figure 6G-I, arrowhead and dashed arrow, respectively). Interestingly, *piwi* transcripts were also detected in more mature cyst cells associated with elongated and polarized spermatids (Figure 6G, solid arrow), highlighting the differences between active transcription detected by snRNA-seq and perdurance of cytoplasmic RNA detected by FISH.

Both *tj* and *eya* mRNA expression was detected in cluster 58, but onward *tj* mRNA was abruptly down regulated while *eya* transcript expression increased. We surmise this marks the transition to cyst cells associated with spermatocytes (Figure 6D,J,V), since Eya protein is known to accumulate in cyst cell nuclei from late stage spermatogonia to spermatocytes (Fabrizio et al., 2003). FISH confirmed the *eya* pattern (Figure 6K, arrowhead and dashed arrow), while also revealing accumulation of *eya* transcript in cyst cells associated with post-meiotic spermatids (Figure 6L, solid arrow).

Intriguingly, the cyst lineage bifurcates after cluster 58, with clusters 77, 65, and 98 successively in one arm and 47, 104, and 88 in the other (Figure 6C,D). This might be due to the onset of differentiation of head versus tail cyst cells, and would represent the first hint at when this occurs in the lineage. Identification and characterization of genes differentially expressed within the split could reveal whether cyst cells specific to a given arm of the lineage govern different properties of spermatocyte-containing cysts.

Expression of *Amphiphysin* (*Amph)* supported the conclusion that the bifurcation in the cyst cell lineage after cluster 58 represents cyst cells associated with spermatocytes. *Amph* mRNA was high before the bifurcation and persisted at lower levels in the two arms of the split, dropping substantially by cluster 74 (Figure 6M,V). Expression of a protein trap confirmed that *Amph* protein levels were high in SgCCs and ScCCs (Figure 6N, arrowhead and dashed arrow, respectively) and declined significantly in cysts containing early spermatids (data not shown). It is intriguing that the snRNA-seq and protein trap indicate that Amph expression is strongest in early cyst cells, even though it encodes a BAR domain protein required to form the actomyosin clamp that maintains head cyst cell membrane integrity as these cells wrap around spermatid heads late in spermatogenesis (Kapoor et al., 2021).

519 Branches of the cyst lineage rejoin at cluster 74 implying a transition to a common
520 transcriptional state. Interestingly, comparison of *Akr1B* vs. *Amph* suggests that cluster 74
521 contains cyst cells associated with early or elongating spermatids. Akr1B transcripts were
522 elevated in both arms of the split through to cluster 74 (Figure 6 - figure supplement 1G) while
523 *Amph* expression had decreased by cluster 74 (Figure 6M,V). Analysis of a *Akr1B::GFP* protein
524 trap confirmed its expression in cyst cells associated with elongating spermatid cysts (SpCC)
525 (Figure 6 - figure supplement 1H,I, arrows). Thus, it appears that, with respect to the
526 transcriptome, a developmental transition occurs within the cyst lineage as these cells mature
527 from support of spermatocytes to early spermatid cysts.

528 After cluster 74, the lineage again splits, with marker analysis suggesting that this correlates
529 with differentiation of late stage head cyst cells (HCC, clusters 69, 79, 68) versus tail cyst cells
530 (TCC, clusters 57, 80, 84, 72; Figure 6A,C,D). None of the clusters along either late branch were
531 enriched for *eya* (Figure 6J,V). However, *Neprilysin-4* (*Nep4*), a metalloprotease involved in male
532 fertility (Sitnik et al., 2014), was upregulated in both late branches (Figure 6P,V), and FISH
533 confirmed *Nep4* expression in late HCCs and TCCs associated with fully coiled spermatids
534 (Figure 6Q, arrow and arrowheads, respectively). Intriguingly, the snRNA-seq data showed
535 expression of the E-cadherin *shotgun* (*shg*) throughout the cyst lineage, with the notable
536 exception of cluster 68 (Figure 6A,R,V). Consistent with this cluster representing late HCCs, FISH
537 revealed higher levels of *shg* in late TCCs than in late HCCs (Figure 6S, arrowhead and arrow,
538 respectively). Conversely, the snRNA-seq data showed that *geko*, an olfactory gene not studied
539 in the testis (Shiraiwa et al., 2000), was upregulated both in cyst cells associated with
540 spermatocytes and in part of cluster 68 (Figure 6A,T,V). In fact, higher resolution (Leiden 8.0)
541 analysis divided cluster 68 into nuclei either enriched or not for *geko* (data not shown). Although
542 FISH for *geko* revealed expression in cyst cells associated with spermatocytes and elongating
543 spermatid cysts throughout the testis (Figure 6U), close inspection of the testis basal region
544 showed high expression in HCCs (Figure 6U', arrows) and lower expression in TCCs (Figure
545 6U,U', arrowhead) as predicted by the UMAP (Figure 6T). Exploring the HCC and TCC clusters
546 further will be revealing given the unique roles played by these cells during spermatid retraction
547 and coiling (Figure 6O).

The hub: architectural organizer and key signaling center

The hub is a small group of somatic, epithelial-like cells at the testis apex that acts as a niche, providing signals that maintain GSC and CySC fate (Hardy et al., 1979; Kawase et al., 2004; Kiger et al., 2001; Leatherman and DiNardo, 2010; Shivdasani and Ingham, 2003; Tulina and Matunis, 2001). Initial marker analysis suggested that the hub maps to cluster 90. However, only 79 of these 120 nuclei clustered together, while other members of cluster 90 were dispersed (Figure 7 - figure supplement 1A). Additionally, the outcast nuclei either expressed germline genes such as *Rbp4, zpg, p53*, and *vas* (Figure 7 - figure supplement 1B-E) or did not consistently express signature genes known to be enriched in hub cells (Figure 7A-D, dashed red circles), strongly suggesting they differ transcriptionally from the 79 tightly clustered nuclei. Consequently, we pared cluster 90 down to 79 definitive hub nuclei (see Materials and Methods).

The snRNA-seq data show that hub nuclei express genes involved in signaling as well as markers common in epithelial cells. For example, *upd1* and *hedgehog* (*hh)* are upregulated, consistent with the hub's role in stem cell maintenance (Figure 7A,B,K) (Amoyel et al., 2013; Kiger et al., 2001; Michel et al., 2012; Tulina and Matunis, 2001). Additionally, hub cells are enriched for proteins implicated in junctional complexes, including factors such as Fasciclin III (Fas3), E-Cadherin (Shg), N-Cadherin (CadN), Discs large (Dlg1), and Cheerio (Cher; an orthologue of Filamin) (Boyle et al., 2007; Le Bras and Van Doren, 2006; Brower et al., 1981; Papagiannouli and Mechler, 2009; Tanentzapf et al., 2007). In agreement with this, hub nuclei exhibited significant expression of these markers (Figure 7C,D,K).

The definitive identification of hub nuclei allowed analysis for upregulated genes ($log_2FC \geq 1$, compared to the full testis plus seminal vesicle dataset; Figure 7 - source data 1) as new candidate hub markers. One such gene encodes the transcription factor Tailup (Tup, also known as Islet (Boukhatmi et al., 2012; She et al., 2021; Thor and Thomas, 1997) (Figure 7E). Indeed, a Tup::GFP transgene showed strong protein expression marking hub nuclei at the apex of adult testes (Figure 7F-F'''). This is consistent with recent evidence that Tup is expressed in and required for niche organization in the male embryonic gonad (Anllo and DiNardo, 2022; Anllo et al., 2019).

Figure 7

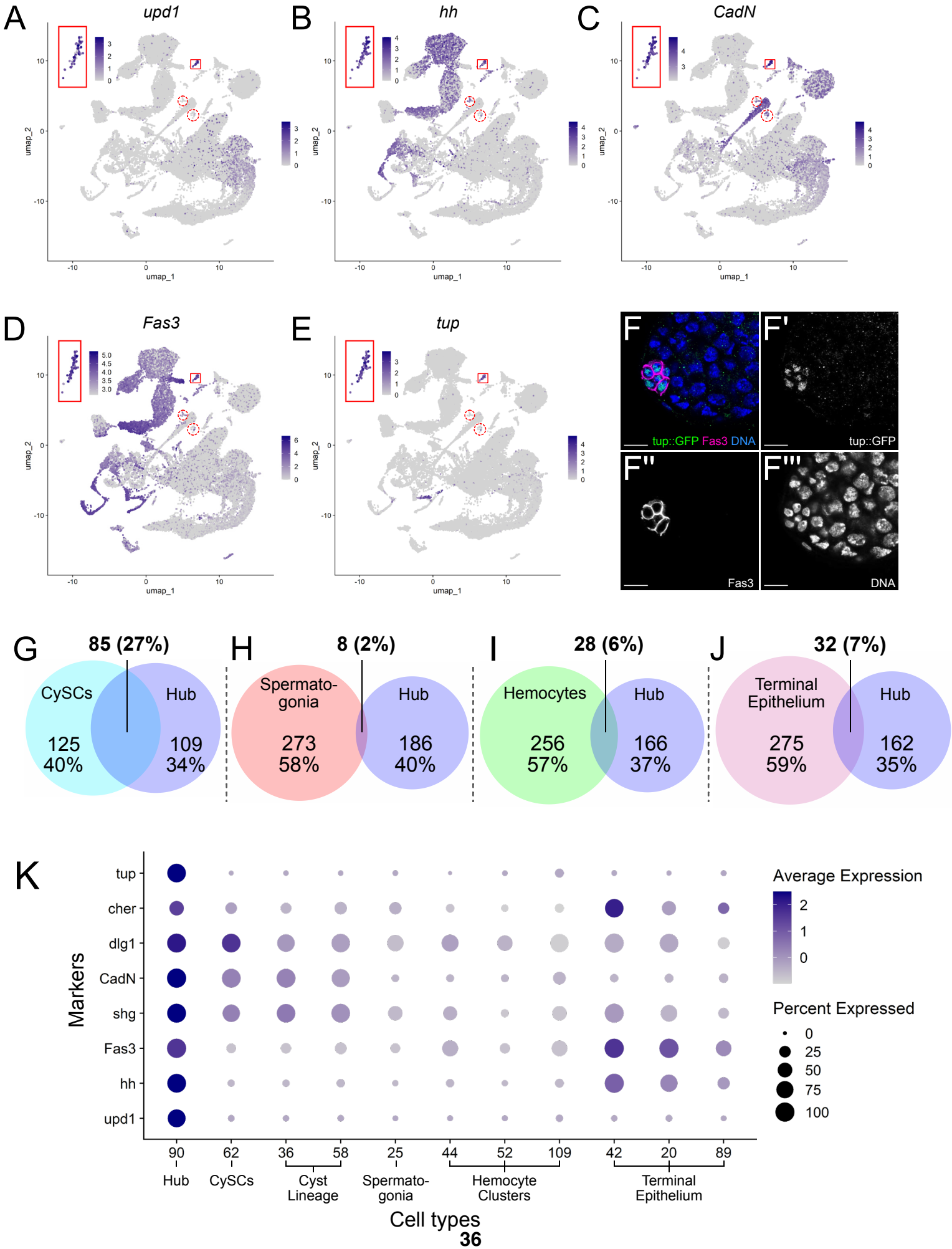
A
upd1
B
hh
C
CadN
D
Fas3
E
tup
umap_1
umap_2
F
tup::GFP Fas3 DNA
F'
tup::GFP
F''
Fas3
F'''
DNA
G
85 (27%)
CySCs
125
40%
Hub
109
34%
H
8 (2%)
Spermato-
gonia
273
58%
Hub
186
40%
I
28 (6%)
Hemocytes
256
57%
Hub
166
37%
J
32 (7%)
Terminal
Epithelium
275
59%
Hub
162
35%
K
Markers
tup
cher
dlg1
CadN
shg
Fas3
hh
upd1
90
62
36
58
25
44
52
109
42
20
89
Hub
CySCs
Cyst
Lineage
Spermato-
gonia
Hemocyte
Clusters
Terminal
Epithelium
Cell types
36
Average Expression
2
1
0
Percent Expressed
0
25
50
75
100

Figure 7 with one supplement

Characteristics of the Hub

(A-E) Expression of the indicated genes (*upd1*, *hh*, *CadN*, *Fas3*, *tup*) projected onto the testis snRNA-seq UMAP with the 79 definitive hub nuclei outlined (small red box). Color intensity corresponds to expression level, shown as normalized average logFC. A reprojection of hub nuclei is shown for each panel (larger red box) with its own key for expression. Red dashed circles contain non-hub nuclei of cluster 90 (see text and Figure S5). **F-F''')** Apical tip of adult testis carrying a Tup::GFP fusion transgene revealing expression largely restricted to hub nuclei delimited by Fas3 (magenta). Nuclei (blue). Scale bar is 10μm. **G-J)** Paired Venn diagrams, comparing up-regulated genes in the hub vs. clusters containing either CySCs, spermatogonia, hemocytes or terminal epithelial cells. Overlap in upregulated genes greatest between Hub and CySCs. In each pairing, circle size reflects the number of genes compared for each cluster. Genes are listed in Figure 7 - source data 1; the specific genes for hub vs. CySCs in Figure 7 - source data 2. **K)** Dot plot of expression of selected genes comparing hub to CySCs, the early Cyst lineage, Spermatogonia, Hemocytes, and Terminal epithelium. (see also Figure 7 - figure supplement 1).

Previous lineage-tracing showed that hub cells and CySCs derive from a common pool of gonadal cells during embryogenesis (Le Bras and Van Doren, 2006; DeFalco et al., 2008; DiNardo et al., 2011). Comparison of genes up-regulated in hub cells with those up-regulated in CySCs strongly reflects this developmental relatedness. Hub and CySC (cluster 62) nuclei share 27% of their up-regulated genes, likely reflecting their embryonic co-origin (Figure 7G, Figure 7 - source data 2). In contrast, the fraction of shared upregulated genes was much lower between the hub and several lineally and functionally distinct cell types, including spermatogonia, hemocytes and terminal epithelia (Figure 7 H-J). Supporting this, several genes up-regulated in the hub are also highly expressed in the CySCs and the cyst lineage, but much lower in spermatogonia and hemocytes (Figure 7K). The transcriptional similarity observed in the adult cell types could account for the ability of hub cells to replenish CySCs after drastic injury, as well as explain the shift of one lineage toward the other when specific gene functions are compromised (Greenspan et al., 2022; Herrera et al., 2021; Hétié et al., 2014; Okegbe and DiNardo, 2011; Voog et al., 2014).

Epithelial Cells of the Testis Organ

A key role of the terminal epithelial cells (TE) is to anchor the head end of elongated spermatid bundles at the base of the testis during individualization and coiling (Figure 6O) so that the sperm are positioned for release into the seminal vesicle (SV). Marker gene analysis suggested that both the TE and SV reside in the “mermaid” of the UMAP (Figure 1B, 8A). snRNA-seq showed enrichment for *hh* in two broad areas of the UMAP (Figure 8B; Figure 8 - figure supplement 1A), while FISH showed *hh* RNA in TE and SV cells (Figure 8C, arrowhead and arrow, respectively). *Metallothionein A* (*MtnA*) was most highly upregulated in the lower clusters enriched for *hh* (Figure 8A,B,D; Figure 8 - figure supplement 1B; clusters 42, 20), with colorimetric ISH confirming strong expression of *MntA* in the TE (Figure 8E, arrow). The SV marker *Neprilysin-5* (*Nep5;* Sitnik et al., 2014), confirmed by FISH to be expressed in SV, was upregulated in the uppermost clusters (Figure 8F,G, arrow; Figure 6 - figure supplement 1C; clusters 1, 4, 7, 9, 29, 32, 34, 93). Although they encode nearly identical proteins, *Nep4* and *Nep5* are expressed in different cell types of the adult testis (HCC/TCC and SV, respectively; Figure 8H). Note that while the TE and SV each map as a single-block cluster at lower clustering resolution (Figure 2 figure supplement 1B), the appearance of multiple clusters for each cell type at higher resolution

Figure 8

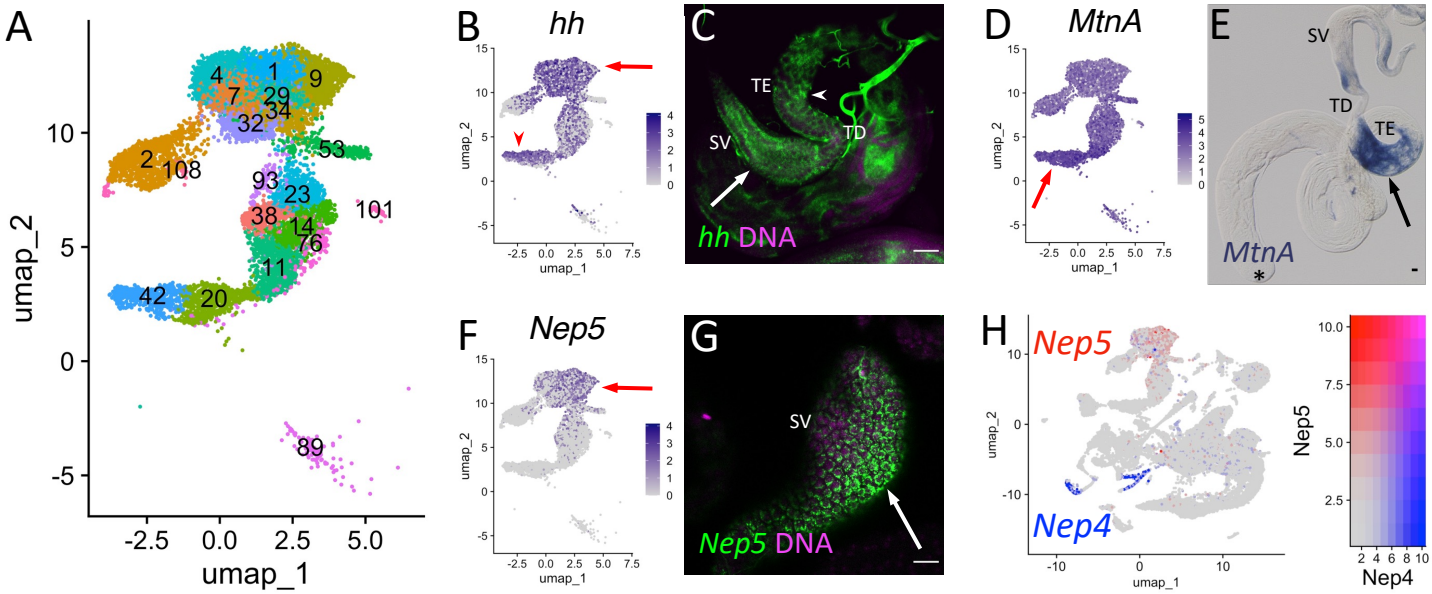
A
B
hh
C
TE
SV
TD
hh DNA
D
MtnA
E
SV
TD
TE
MtnA
F
Nep5
G
SV
Nep5 DNA
H
Nep5
Nep4
umap_1
umap_2
Nep5
Nep4

Figure 8 with one supplement

Characteristics of supporting epithelia

A) UMAP of non cyst cell lineage epithelial cells of the testis from the FCA snRNA-seq data with Leiden 6.0 clusters. Note: identity of cluster 89 remains undefined. **B - G)** In these panels, a UMAP is compared to a set of (F)ISH images. For each gene comparison, arrows and/or arrowheads point out the same cell type in the UMAP and its corresponding FISH image. **B)** *hh* mRNA expression projected on the UMAP. **C)** FISH of *hh* mRNA (green) and DNA (magenta) showing the base of the testis including the TE (arrowhead), testicular duct (TD), and SV (arrow). **D)** *MtnA* mRNA expression projected on the UMAP. **E)** Colorimetric *in situ* hybridization of *MtnA* mRNA (blue) in an entire testis. **F)** *Nep5* mRNA expression projected on the UMAP. **G)** FISH of *Nep5* mRNA (green) and DNA (magenta) showing the SV. **H**) *Nep4* (blue) and *Nep5* (red) mRNA expression projected on the UMAP with corresponding heatmap. Arrows and arrowheads point to corresponding cells on UMAPs and stained tissues. Asterisk denotes hub. Bars: 20μm. (see also FIgure 8 - figure supplement 1).

suggests notable transcriptional heterogeneity within both cell types (Figure 8A). Thus, epithelial cell types in general represent an underexplored area in testis biology.

Discussion

Study of the *Drosophila* testis has had great impact on reproductive biology and on understanding stem cell-niche interactions, developmentally regulated cell cycles and cell type specific cellular morphogenesis. Against this foundation, examining single cell and single nuclear RNA-seq has revealed several notable features. First, in gene expression space, each stem cell-based lineage was geographically isolated from the other, reflecting their distinct lineage identity. Second, the individual cells within each stem cell lineage are essentially arranged in strings, due to progressive changes in gene expression during differentiation. Third, a UMAP for each lineage revealed complexities along its trajectory that reflect both known intricacies of development within each lineage, as well as previously unappreciated gene expression dynamics. Fourth, in contrast to the two stem cell lineages, terminally differentiated cells generally clustered into discrete groups, as expected. Finally, the comparison of single cell and single nucleus datasets proved particularly revealing of dynamic developmental transitions in lineage differentiation.

Germline and soma map to distinct gene expression domains

While *Drosophila* spermatogenesis relies on two separate stem cell lineages, the progeny of each lineage associate intimately with each other, cooperating at multiple points during differentiation to produce functional sperm. Despite their physical association, in gene expression space the two lineages lie well-separated. This is not a surprise, since the lineages are specified independently during embryogenesis in space and time, as well as by different gene regulatory circuits. Such separation between germline and supporting soma is also observed in the scRNA-seq from the *Drosophila* ovary and murine testis (Green et al., 2018; Rust et al., 2020).

Accurate pairing of each germline cluster with a somatic cluster representing its interacting partner could facilitate identification of the underlying cell signaling circuits that form the basis for cooperation between the lineages at various points along their differentiation trajectory. We are able to highlight some likely pairing assignments due to the extensive knowledge of *Drosophila*

spermatogenesis and testis biology. For example, the CySC cluster (62) likely associates directly with germ cells in cluster 25, while cyst cell lineage clusters 36 and 58 likely associate with later spermatogonia (cluster 22). Other associations are also suggested by the data (Figure 6D) with more remaining to be defined. The transcriptome in these pairings can be mined to identify candidate signaling pathways by recently developed tools, such as FlyPhone (Liu et al., 2022).

Stem cell lineages appear as strings along their differentiation path

The data highlight how tissues maintained by stem cell lineages display a characteristic geography in gene expression space. The UMAP reveals these lineages to be arranged largely in strings, due to progressive changes in gene expression. The linear arrangement is strongly supported by trajectory inference for both the sc- and sn-RNA-seq datasets (see also Li et al., 2022). This arrangement might be diagnostic of at least some stem cell lineages, as it is observed to a degree in germline data from murine testes, in murine small intestine (Green et al., 2018; Haber et al., 2017), and in the follicle cell lineage in the *Drosophila* ovary (Li et al., 2022; Rust et al., 2020). While in some tissues maintained by stem cells, such an arrangement is made apparent only by trajectory inference, in the *Drosophila* testis it is apparent in the UMAP representing gene expression space.

Additionally, even with progressive changes in gene expression along their respective trajectories (Figures 2L, 6V), cells in these strings nevertheless can be sorted into clusters. The extensive study of germline and somatic testis biology provided excellent markers, which allowed assignment of cell stage identity with high confidence for many of these clusters. These assignments provide abundant opportunities to identify new, *in vivo* stage-specific markers to test for function in each stem cell lineage.

Each stem cell lineage exhibited complexities, revealing known and previously unappreciated expression dynamics

In the testis, differentiation proceeds stepwise from the apical tip of the tubule. It is tempting to equate this progression with the arrangement of cell states revealed in the UMAP. However, the UMAP represents gene expression space and not physical space. This means that

a stage characterized by dramatic changes in transcription in a differentiating lineage, while localized to a very small region within the organ, might be spread out in a thin stream in the UMAP. An example is seen in early spermatocytes, from completion of premeiotic S phase through to apolar spermatocytes (Fuller, 1993). Physically located in a narrow band next to the spermatogonial region in the testes, nuclei at these stages extend across much of the lower region of the germ cell UMAP (Figure 2A). A reciprocal case is highlighted by early spermatids, which have very low levels of transcription and thus show very low UMI values. These cells are clustered together in the UMAP, even though the cells are undergoing dramatic changes in morphology easily visible by microscopy (Fuller, 1993).

For the soma, the complexity observed within portions of the cyst lineage was a surprise. Head and tail cyst cells execute very different roles for the spermatid bundles with which they associate. Not surprisingly, the distinction between head and tail cyst cells is clear late in the differentiation process in the UMAP, when the two cell types have very different morphologies. Our analysis confirmed that both head and tail cyst cells are derived from the same progenitor population (Figure 6D). However, the somatic clusters show complex intertwining before they eventually resolve to generate the two lineages. Interestingly, this complex tangling seems to coincide with the stages of spermatid development where there already is clear polarization in the architecture of the bundle (Figure 6D). Only by reprojecting this lineage, purposefully preserving an extra dimension, could we infer the trajectory properly, discerning a split and then a merge in expression profiles that tracked with cell identity. The initial split in the cyst lineage, as well as the subsequent and transient merge followed by a new split, suggests an interesting sequence of transcriptional cell states within this key supporting lineage.

Differentiated cells map as discrete groups

Whereas the two stem cell lineages each appear as strings reflecting progression in their gene expression patterns, terminally differentiated cell types appear as more discrete patches in the UMAP (Figure 1F). This was the case for differentiated cell types that are an integral part of the testis, such as the hub and terminal epithelia, as well as for cell types that associate with the testis but are structurally distinct, such as the seminal vesicle. Even within a patch, however,

691 increasing cluster resolution reveals complexity in cell type identity. For example, the snRNA-seq
692 identifies a 'muscle' group (Figure 1B, 'mc') that is composed of several different Leiden 6.0
693 clusters (Figure 2 - figure supplement 1, compare A with B). Perhaps the clusters reflect different
694 muscle cell types, for example those covering the testis tubule vs. the seminal vesicle (Susic-
695 Jung et al., 2012). Likewise, different clusters that comprise 'seminal vesicle' may represent
696 distinct portions of the structure, such as entry and exit points (Figure 8A).

697 **The value of sn- versus sc-RNA-seq comparison**

698 When carried out on the same tissue, single nucleus RNA-seq is typically comparable to
699 single cell RNA-seq, with very high percent similarity in gene identification (McLaughlin et al.,
700 2021). In the *Drosophila* testis, this was largely the case for germ cells early in the differentiation
701 lineage (Figure 4 G and H). In contrast, comparing these two approaches for later stage germ
702 cells revealed a striking difference, reflecting an important aspect of testis biology. Our data show
703 that directly comparing sn- to scRNA-seq can highlight cases where mRNAs are expressed at an
704 early developmental stage (e.g. in spermatocytes) then stored for later use (e.g. in spermatids,
705 where mRNAs may be utilized temporally). snRNA-seq likely reports mRNAs being actively
706 transcribed at a given developmental time and therefore may be more sensitive to dynamic
707 changes in transcription than scRNA-seq. Thus snRNA-seq may be a better approach for
708 mapping changes in cell state, for example, during embryonic development or differentiation in
709 stem cell lineages. Data from scRNA-seq, by contrast, may be strongly influenced by mRNAs
710 perduring in the cytoplasm from earlier time points, as well as mRNAs no longer being actively
711 synthesized but purposefully stored for later usage. Thus, while snRNA-seq reveals gene
712 expression dynamics through *active* transcriptional changes, scRNA-seq can capture post-
713 transcriptional gene regulation, as is required by transcriptionally silent cells like early spermatids.

714 Additionally, as we show here, comparison between the two approaches was key to
715 revealing programs where perdurance of mRNAs plays an important role. Cytoplasmic storage
716 of transcripts expressed at an earlier stage to be used later is especially predominant during
717 oogenesis and spermatogenesis. Many mRNAs expressed during oogenesis are stored in the
718 cytoplasm in a translationally silent state, to be recruited for translation in the early embryo

(Jenkins et al., 1978). This is especially important in organisms with large, yolk-rich eggs, in which transcription from the zygotic genome is delayed until after several rounds of mitotic divisions. In the male germ line as well, where transcription ceases during spermiogenesis as the nucleus compacts, many mRNAs expressed at earlier stages are stored in the cytoplasm, initially translationally repressed, then recruited for translation during spermatid morphogenesis. In both cases, perdurance of the mRNAs in the cytoplasm after transcription has shut down is important to allow subsequent stages of development and differentiation to take place, and recruitment of different mRNAs for translation may play important roles in temporal control of morphogenetic events.

It is also notable that just 18 of the spermatid transcribed genes encode proteins detected in the mature sperm proteome (Wasbrough et al., 2010). While this might be due to limited sensitivity in proteome detection, alternatively, many may play roles in spermatid development but not mature sperm function. Examples could include regulating or mediating spermatid elongation, the histone-to-protamine transition, or individualization, as is the case for *soti* (Barreau et al., 2008; Kaplan et al., 2010). A further twenty of the 22 cytoskeletal or motor-related genes transcribed in spermatids (see Figure 5 - source data 1 for functional classes of the spermatid transcribed genes) have predicted functions in microtubule assembly, flagellar axoneme assembly, axonemal dynein regulation or microtubule transport, consistent with roles in elongating and assembling the 1.8mm sperm flagellum and transporting cargos within this large cell (Ghosh-Roy et al., 2004; Noguchi et al., 2011; Tokuyasu, 1975). The set of identified lipid synthesis, lipid transfer and membrane trafficking genes could contribute to membrane addition at the distal (growing) ends to facilitate cell elongation (Ghosh-Roy et al., 2004). Finally, genes encoding RNA binding proteins could regulate transcript localization or translation in the increasingly long spermatid cells, as polarized mRNA localization by RNA binding proteins such as Orb2 (localizing *aPKC* and *orb2* mRNA) and Reptin and Pontin (localizing axonemal dynein mRNA) has been observed and shown to be important for sperm maturation (Fingerhut and Yamashita, 2020). Whether and how many other mRNAs are localized to the growing flagellar tip in spermatids remains to be studied.

Use as a resource

With the transcriptional profiling of over 44,000 nuclei isolated from testis and associated supporting tissues, we have connected differentiation events throughout the germline and somatic lineages, capitalizing on the extensive literature on *Drosophila* testis biology. The expectation is that this will be a foundational resource for the field. Several other *Drosophila* RNA-seq and scRNA-seq efforts have been reported (Gan et al., 2010; Hof-Michel and Bökel, 2020; Mahadevaraju et al., 2021; Shi et al., 2020; Vedelek et al., 2018; Witt et al., 2019). Since each approach has different relative strengths and limitations, the foundation we have laid with the scRNA-seq and snRNA-seq datasets described here should assist others in comparisons with more stage-restricted transcriptome analyses. More broadly, the data presented here, in their easily shared formats, should enable a deeper exploration of the conserved aspects of germline and support cell biology during *Drosophila* and mammalian spermatogenesis.

Materials and Methods

Drosophila lines

For snRNA-seq, testes and attached seminal vesicles were dissected from 0-1 day old w^{1118} males and processed as described in (Li et al., 2022). For scRNA-seq, testes alone were dissected from 1-5 day old Oregon-R males. Oregon-R testes were also used for *in situ* hybridization of *aub* and *fzo* (Figure 2). y^1w^1 flies were used for smFISH in Figure 5. Amph::GFP (CPTI-002789), piwi::GFP (CPTI-003588), Akr1B::GFP (CPTI-002728), CG3902::GFP (CPTI-100001) and Tup::GFP (BDSC line 81278) were from CPTI and Bac collections (Kudron et al., 2018; Lowe et al., 2014). $comr^{z2\text{-}1340}$ homozygotes and w^{1118} were used for colorimetric *in situ* hybridization.

Testis squashes and analysis of expression of fluorescent fusion proteins

Testes from transgenic flies of the YFP CPTI collections were dissected in testis buffer (183mM KCl, 47mM NaCl, 10mM Tris pH6.8), cut open using tweezers and gently squashed on a glass

slide by application of a coverslip. Testis squashed preparations were imaged live in sequentially captured images by phase contrast and epifluorescence microscopy using an Olympus Bx50 microscope, with 20x, 0.60 NA, 10x, 0.30 NA, or 40x, 0.75 NA UPlanFl objectives and either a JVC KY F75U or a Hamamatsu Orca-05G camera.

For Tup::GFP analysis, testes were dissected from BAC transgenic flies, fixed in 4% paraformaldehyde for twenty minutes, and blocked in 3% bovine serum albumin, 0.02% sodium azide, 0.1% Triton X-100 in phosphate-buffered saline for one hour. After a one hour wash with PBX (0.1% Triton X-100 in 1X phosphate-buffered saline, pH 7.4), testes were incubated overnight at 4°C with antibodies to GFP (Abcam 13970; 1:10,000) and Fasciclin-III (Developmental Studies Hybridoma Bank 7G10; 1:50). After washing with PBX testes were treated with goat anti-chicken AlexaFluor 488 (Invitrogen A, 11039; 1:200), goat anti-mouse AlexaFluor 568 (Invitrogen A11004; 1:100), and DAPI (Millipore Sigma 1023627600; 1:1,000) for two hours. After final washes in PBX, testes were mounted in VectaShield (Vector Labs H-1000), and images were captured at 63X, NA 1.4, on a Zeiss LSM800 confocal microscope.

RNA in situ Hybridization

For *in situs* presented in Figures 2 and 4:

aub (forward primer 5'-CCTGGGCGGCTACATCTT-3'; reverse primer 5'-GCGCAGATTTCGACTCGG'-3), *kmg (*forward primer 5'-TGCCTCTATGCCTCACGC-3'; reverse primer 5'- GCGCCTACCGGTCTCATC-3''*), fzo* (forward primer 5'-GGCATCCAAACTCTCGCG-3';

reverse primer 5'-TGTCGCAACTGGAGCTCA-3') were amplified by PCR on cDNA from Oregon-R Drosophila Testes. Using TA cloning (Promega, "Easy-T" Cloning), the resulting amplicons were cloned into th pGEM vector (Promega). Subsequent PCR added a T7 binding site (5'-GAAGTAATACGACTCACTATAGGGAGAGGG-3') upstream of the amplicon. The resulting plasmids then served as templates for *in vitro* transcription with Digoxigenin (DIG)- and fluorescein isothiocynate (FITC)-labeled ribonucleotides to generate labeled single-stranded antisense riboprobes.

Testes were isolated and fixed in 4% formaldehyde for 30-60 minutes, dehydrated into methanol and stored at -20°C for up to 1 month. After rehydration in PBS + 0.1% Triton-X100, testes were permeabilized with 4 ug/ml Proteinase K for 6 minutes and washed with Pre-Hybridization solution (50% deionized formamide, 5x SSC, 1mg/ml yeast RNA, 1% Tween-20) for up to 2 hours at 56°C. Testes were incubated overnight at 56°C with probes diluted 1:800 in Hybridization solution (50% deionized formamide, 5x SSC, 1 mg/mL yeast RNA, 1% Tween-20, and 5% Dextran Sulfate). After washes in Pre-Hybridization solution, 2x SSC, and 0.2x SSC, then PBS+0.1% Triton-X100, samples were blocked for 30 minutes in 1% Roche Western Blocking Reagent prior to incubating overnight at 4°C with either anti-FITC with horseradish peroxidase conjugate (Roche) at a 1:2000 concentration or anti-DIG- with horseradish peroxidase conjugate (Roche) at a 1:1500 concentration in 1% Roche Western Blocking Reagent. Fluorescent tyramide development and amplification were performed by first placing the testes for 5 min in borate buffer (0.1M boric acid, 2M NaCl, pH 8.5), followed by 10 min in borate buffer with rhodamine (1:1000) or fluorescein (1:1500) tyramide, and 0.0003% hydrogen peroxide. After development, peroxidase activation was performed in a 1% sodium azide solution for at least 1h, followed by antibody labeling for the second probe. Coverslips were mounted in Vectashield with DAPI (Vector Labs). Fluorescence image acquisition was performed on a Leica Stellaris Confocal microscope using a 63X oil-immersion objective (NA = 1.4).

For *in situs* presented in Figures 5, 6, and 8:

Fixation and hybridization for FISH was as described for Figures 2 and 4, with minor modifications as described (Wilk et al., 2017). Briefly, these include using a cold acetone permeabilization step and 0.3% Triton X-100 instead of Proteinase K for improved tissue permeabilization, and DIG-labeled probe detection via tyramide amplification. DAPI (4" ,6-diamidino-2-phenylindole; Sigma, cat. no. D-9542) was used at 1 ug/ml to reveal nuclei. For detection of *piwi*, *eya*, *f-cup*, *loqs* and *geko* transcripts, RNA probes were transcribed from the BDGP DGC library plasmid clones GM05853, GH05272, GH09045, RE14437 and RE30284, respectively using T7 RNA

polymerase. For *hh* and *Nep5*, templates were made by PCR from genomic DNA using the following T7 and T3 promoter-containing primers:

Hh last exon:

Forward: GTAATACGACTCACTATAGGGAGACCACTGCCGATTGATTTTCTCAGG

Reverse: AATTAACCCTCACTAAAGGGTTGTGGAGATCGTGTTTTGAGCAT

Nep5 exon 6:

Forward: GTAATACGACTCACTATAGGGAGACCACGGGGAAATCCGATAAAGCTC

Reverse: AATTAACCCTCACTAAAGGGTTGTATCTGCAGAACCAAACTGAC

For colorimetric *in situ* hybridisation in Figure 3, 8 and Figure 3 - figure supplement 1

Probe preparation and *in situ* hybridisation were performed as described (Morris et al., 2009). Primers Hml-F ATTTAGGTGACACTATAGAATAAGTGGACCCATGCCAAG and Hml-R TAACCCTCACTAAAGGGTGACCATCATCGCAAATC and. primers MtnA-F ATTTAGGTGACACTATAGAAGCGGTAAGTTCGCAGTC and MtnA-R TAACCCTCACTAAAGGGACATTTATTGCAGGGTGTG were used to amplify 628bp and 443bp fragments respectively from cDNA generated from w^{1118} testes. After re-amplification using primers 5'-SP6 ACGGCAATTTAGGTGACACTATAGAA and 3'-T3 GCAACGAATTAACCCTCACTAAAGGG, and the products served as templates for T3 RNA polymerase to generate dig-labeled single stranded, antisense RNA probes. The probes were hydrolysed for 15 minutes, precipitated and resuspended in 200 µl water. Testes were dissected from young w^{1118} males, fixed in 4% paraformaldehyde for 20-60 minutes, washed in PBS, permeabilised with 50 µg/ml proteinase K for 5 minutes, washed in PBS, then hybridisation buffer (HB: 50% Formamide, 5× SSC, 100 µg/ml denatured sonicated salmon sperm DNA, 50 µg/ml heparin, 0.1% Tween 20, 100 mM citric acid). Probes were diluted 1:100 in HB and testes were hybridized for 16 hr at 65°C. Testes were washed 6x30 min at 65°C in HB, followed by 15 min each step at room temp in 4:1, 3:2, 2:3 1:4 HB:PBST, 2x15 min PBST, then incubated overnight at 4°C in alkaline phosphatase-conjugated anti-digoxygenin antibody diluted 1:2,000 in PBST.

Testes were washed 4x15 min in PBST and finally 3x 5 min HP (100 mM NaCl, 100 mM Tris (pH 9.5), 50 mM MgCl2, 0.1% Tween 20). NBT and BCIP diluted in HP were added as a colorimetric substrate for alkaline phosphatase and color allowed to develop in the dark at room temperature. The testes were washed in PBST, dehydrated through an ethanol series, mounted in GMM, and imaged using DIC microscopy (10x objective) with a JVC KY F75U camera mounted on an Olympus BX50 microscope.

For single molecule FISH presented in Figure 5

smFISH was performed as previously described (Fingerhut et al., 2019). Briefly, testes were dissected in 1xPBS (Invitrogen, AM9624) and fixed in 4% formaldehyde (Polysciences, Inc., 18814-10) in 1xPBS for 30 minutes, washed twice in 1xPBS for 5 minutes each, and permeabilized in 70% ethanol overnight at 4°C. Testes were washed with wash buffer (2x saline-sodium citrate [SSC, Invitrogen, AM9770], 10% formamide [Fisher Scientific, BP227]), and then hybridized overnight at 37°C in hybridization buffer (2xSSC, 10% dextran sulfate [Sigma-Aldrich, D8906], 1mg/mL yeast tRNA [Sigma-Aldrich, R8759], 2mM Vanadyl Ribonucleoside complex [New England Biolabs, S1402S], 0.5% BSA [Invitrogen, Am2616], 10% formamide). Following hybridization, samples were washed twice with wash buffer for 30 minutes each at 37°C and mounted in Vectashield with DAPI (Vector Laboratory, H-1200, Burlingame, USA). Images were acquired using an upright Leica Stellaris 8 confocal microscope with a 63X oil immersion objective lens (NA = 1.4) and processed using ImageJ and Adobe Photoshop software (National Institutes of Health, Bethesda, USA).

Fluorescently labeled probes were added to the hybridization buffer to a final concentration of 100nM. Probes against *soti* and *wa-cup* transcripts were designed using the Stellaris® RNA FISH Probe Designer (Biosearch Technologies, Inc., Novato, USA) available online at www.biosearchtech.com/stellarisdesigner.

Probe Target	Fluorophore	5’-Sequence-3’

wa-cup	Quasar® 670	cttccgataagctcatttgg,	ccgctgttgggtgaaaaaga,
		ccagagcgctgttgaaatac,	gagctctttcattgaacgga,
		atcgatcttttcagctgact,	ctttcggctcatcaacagat,
		gactgacattgggattggtt,	tacagagcatcgcagacttc,
		gaatcttccaagcgattgga,	ccggagctaaatcgctttaa,
		tgagacggtcgagaacagga,	gacatggtggtatcatctga,
		aactagccatcatgcgattg,	gtatccttaatatccttggg,
		gttttccattatgctaacca,	agtggggacaaatgggtttc,
		ttaaaatgccttttcgcct,	ccagcatttgttcagatacg,
		tcgcagtgtcttcagaaagg,	gacttttgcaatgcttggg,
		catcagtttgcccaaatact,	tgcgttccgctttataattg,
		taaggcgtacatgggacttc,	ctcgttgggatatttctgtt,
		ctcccggtgcttattataaa,	gtctggtactgaatgcgata,
		atgctgcgcagaatcttgaa,	gttctccaactcgaattagc,
		cccatgacttcctcaataaa,	cgtcttgatggtgacatagt,
		aaatttccacggcattacgc,	aatgcgagctaaacccaagt,
		agacagtcatattgctggga,	gtgttagcagacgttgtttg,
		actcgttcgttttgtctttg,	gtagccgatctggttatatt,
		ttaaaatgctccgctttggg,	atacgattttccagtcggac,
		gttcaatgtgatactcggca,	aattcgtgcagtagataggc,
		acaattcagatgctcttggg,	ctccatataacactcttgca,
		gccttgcatataaccatgag,	taagcacaggtcaaggttct,
		ctcctccgcattaactttaa,	tgagccaaacttttgtctct,
		ctgatcgttgctttggaaca,	taatttggttgcgatcctca

soti	Quasar® 570	ctctcgacgaggtaatttg,	tccgtgtagtacgtccat,
		gctcatcgtacagatcgt,	ccgactcgatcgattagc,
		atcttcattcaccgcgtc,	tgtccaagtcatcgccag,
		tgctgtccatcctccaat,	tgacgattgactcccagg,
		gtccaggagtatgtccat,	caacggtggctcttgagg,
		ctccttgcgccggaaaaa,	acgtggtggtccatttgg,
		aacttcgtttcttccgcc,	ggagtgggtttggtcata,
		ctcctgactttggcatgg,	ttaggaggcacatctccg,
		attgccctcgtgacactg,	atcctcgcgaacgtgacg,
		caaagtactcgcctcgct,	gggtagttctgactggtc,
		tggcagacccataccatt,	agaactgaccccaatgct

884

885 ***Preparation of samples for snRNA-seq***

886 FACS-sorted nuclei were obtained from hand dissected, 0-1 day-old adult testes (plus seminal
887 vesicles) and processed as described by the Fly Cell Atlas project (Li et al., 2022). Data from
888 44,621 sequenced nuclei passed quality control metrics. The raw data are publicly available
889 (https://www.ebi.ac.uk/arrayexpress/experiments/E-MTAB-10519/).

890 ***Importing FCA data into Seurat***

891 The "Testis, 10X, Relaxed" loom file (https://flycellatlas.org/; Li et al., 2022) was imported into
892 Seurat 4.0.5, and a standard pipeline run on the resulting Seurat R object to normalize and scale
893 the data (NormalizeData, FindVariableFeatures, and ScaleData). The loom file had already been
894 filtered with nuclei expressing less than 200 genes or exceeding 15% mitochondrial content
895 removed and genes not expressed in at least 3 nuclei removed. We chose to use the relaxed
896 rather than a '10X, Stringent' testis loom file due to the particular biology of the testis. Testis
897 germline cells can express 'somatic' genes (see Results), including the hub cell marker *upd1*. As
898 a consequence, filtering algorithms that generated the stringent dataset led to loss of a
899 documented somatic cell type (the hub), as well as a large number of late spermatocytes. The
900 Fly Cell Atlas website provides links and tutorials to ASAP and SCope, two web-based pipeline

and visualization portals where users can examine the data or re-run analyses (Davie, 2018; Gardeux, 2017). Within the SCope interface, select the 10X > Testis > Relaxed dataset, and Settings > HVG UMAP. The analysis in this paper complements SCope and ASAP with Seurat and Monocle3, two R programming-based tools for single cell analysis (Satija et al., 2015; Trapnell et al., 2014 , Tools for Single Cell Genomics • Seurat; https://cole-trapnell-lab.github.io/monocle3/).

The cluster information contained in the original loom file was preserved in the Seurat object, with clusterings available at increasing levels of resolution (Leiden algorithm, 0.4 to 10). The level of granularity provided by resolution 6.0 was deemed most revealing and is used for most analysis here. The full Seurat Object, FCAloomToSeurat2TFP_Annotations.rds, is available for download at Input Files.

Original cluster 90 was manually split into two in the Seurat Object, FCAloomToSeurat2TFP_Annotations.rds, with one resultant cluster of 79 nuclei definitively established as representing the hub (retaining its cluster number, #90), and the remaining nuclei placed into a new cluster, #111. Venn diagrams were created using Venny 2.1 (Oliveros, J.C. 2007-2015).

In some cases, data were extracted from subsets of the original Seurat object: a germline only subset (Figures 2 through 5), a somatic cyst cell lineage subset (Figure 6), and a subset representing several epithelial cell types of the testis as well as specific additional epithelial cell types (Figure 8). All UMAPs were generated within Seurat using the “DimPlot” function. UMAPs that highlighted particular genes of interest were generated using the “FeaturePlot” function (Figures 1, 2, 3, 5, 6, 7, 8). Dotplots were generated using the “DotPlot” function (Figures 2 through 7).

The testis 10X Relaxed loom file only contains a UMAP reduction projected to two dimensions. To inspect a 3D UMAP representation, the appropriate lineage was isolated and reprojected,

passing the argument 'n.components =3L' to the Seurat function 'RunUMAP' (see cystlineage3Dcode.R code; (Qadir et al., 2020); 10.5281/zenodo.348317). An html version of the resulting 3D representation is available for download at Input Files.

For analysis of heart, Malpghian tubule and male reproductive gland (Figure 3 - figure supplement 1), the appropriate stringent 10X loom file from Fly Cell Atlas was imported into Seurat. Means were calculated for nCount (UMI) and nFeature (gene). Cluster numbers were assigned using the "Annotation" metadata field in each object, and a plot produced for average UMI by cluster number, with dot size reflecting average gene number per cluster.

Graphs generated directly from ASAP were used to produce Figures 3D-E (Gardeux *et al.*, 2017). Continuous Coloring of a Custom Gene Set - Categorical Gene Metadata: _Chromosomes (either X or Y) was used under the Visualization tab. SVGs can be saved directly from the website. The enrichment analysis performed to produce these graphs mirrors Seurat's AddModuleScore function and is detailed in the Materials and Methods of Li et al., 2022 (see header: Metabolic clustering using ASAP).

On occasion, use of an alternative Assay ("log.counts") in the Seurat Object allowed for visualization of low levels of gene expression in spermatocytes. This "log.counts" assay contains a matrix of $\log_2$(counts + 1), or log-transformed raw counts. This was done for plotting or to perform analyses focused on promiscuous expression in spermatocytes (Figures 3F-G, 3J, Figure 3 - figure supplement 1D-G, Figure 3 - source data 1). Figure 3 code describes how this assay was added and shows how to utilize this information when needed.

Cell type-specific transcription factors were taken from Li et al., 2022, Table S3 and are available at Input Files (TFs_list_500.txt). Each gene was classified as being only in mature spermatocytes, both in other cell types and mature spermatocytes, or not in germ line cell types as per assignments in the Fly Cell Atlas Table S3 (Li et al., 2022). Figure 3 - source data 1 was generated by calculating average log-transformed expression of each transcription factor per Leiden 0.4

cluster. Subtracting the value in cluster 3 from that of cluster 2 yielded the upregulation of each gene in mature spermatocytes relative to spermatogonia and early spermatocytes (Figure 3J, Figure 3 - source data 1).

Tissue isolation and cell dissociation for scRNA-seq

The testis dissociation protocol was adapted from Witt et al., 2019. Fresh maceration buffer (10mL Trypsin LE (Gibco) with 20 mg collagenase (Gibco)) was prepared on the day of the dissection. Testes were hand dissected from 1-5 day old male flies in 1x phosphate-buffered saline (PBS), separated from seminal vesicles and transferred immediately into tubes filled with cold PBS, on ice. Testes were kept in PBS for a maximum of 30 minutes. Samples were centrifuged at 135 rcf and the PBS removed and replaced with 400 µL marceration buffer. Testes were incubated in maceration buffer for 30 minutes with gentle vortexing every 10 minutes at room temperature. Following incubation, samples were pipetted up and down for 15 minutes until all visible chunks were gone and the sample was in approximately a single-cell suspension. Sample was filtered through a 35 µm filter into a polystyrene tube, then transferred into a microcentrifuge tube. After the sample was centrifuged at 135 rcf for 7 minutes, the supernatant was removed and the pellet resuspended in 1mL calcium- and magnesium-free Hanks' Balanced Salt Solution (HBSS). The sample was spun a final time at 137 rcf for 7 minutes. All but 50 µL of the HBSS supernatant was removed, and the cell pellet was resuspended in the remaining 50 µL. Cell viability and density was then assayed on a hemocytometer using DIC imaging and Trypan Blue stain.

Library preparation and sequencing for scRNA-seq

Cells were processed using the 10x Genomics Chromium Controller and Chromium Single Cell Library and Gel Bead Kit following standard manufacturer's protocol. Amplified cDNA libraries were quantified by bioanalyzer and size selected using AMPure beads. Samples were sequenced on a NovaSeq SP.

Mapping and preprocessing of scRNA-seq data

Reads were mapped to the DM3 reference genome using the 10X CellRanger pipeline with default parameters. The resulting feature matrix (default output, kept in outs/filtered_feature_bc_matrix, and featuring barcodes.tsv.gz, features.tsv.gz, and matrix.mtx.gz) was read into the R package Monocle3 using load_cellranger_data. The resulting cell data set (cds) object was processed using 100 dimensions, and underwent dimensionality reduction using the UMAP method. Germline cells were identified on the basis of super-cluster (in Monocle3, "partition") identity, with 100 dimensions used to identify partitions. The germline cells were then subsequently clustered using the Monocle3 "cluster_cells" command, with resolution = 0.003.

Trajectory analysis of FCA snRNA-seq data

The publicly available "Testis, 10X, Relaxed" loom file of snRNA-seq data from the Fly Cell Atlas website (https://flycellatlas.org/; 10.1101/2021.07.04.451050) was read into Monocle3, and preprocessed using 50 dimensions. This dimension number was determined empirically as it resulted in connected clusters that represented the primary lineages (germline and cyst). UMAP dimensionality reduction and clustering was performed with a resolution of 0.0002, again determined empirically to represent biologically significant clusters that approximated the original annotation. A trajectory graph was generated from data with "learn_graph". Pseudotime was calculated with "order_cells", with the first (base) node selected as the root in Monocle3's interactive mode. Pseudotime parameters were then subsequently visualized on the original projection by adding a "pseudotime" slot to the FCA Seurat object. "learn_graph" and "order_cells" were likewise run on the scRNA-seq dataset, with the single most base node again selected as the root.

A list of genes that change expression level dynamically along pseudotime was generated from the full join of genes that vary along pseudotime in the single cell and nucleus datasets, according to the graph_test function in Monocle3 (parameters: neighbor_graph = "principal_graph", method = "Moran_I" cores = 4; selected genes with q_value = 0 and morans_I = 0.25). Additionally,

several genes encoding transcripts that were annotated as enriched in late pseudotime in the original FCA paper were added to the analysis. Genes (representing rows on the Figure 4G-H heatmaps) were ordered according to pseudotime point of peak expression averaged between the two datasets. A z-score for each gene expression for each dataset, smoothed across pseudotime using R function "smooth.spline" with 3 degrees of freedom was calculated and the heatmap was generated using the R package ComplexHeatmap.

Aligning trajectories for scRNA-seq and FCA snRNA-seq data by dynamic time warping

The trajectories for the scRNA-seq and snRNA-seq data were aligned on a common "warped" time scale using a Dynamic Time Warping based procedure (adapted from Alpert et al., 2018; Cacchiarelli et al., 2018). The smoothened gene expression (as shown in the heatmaps) for all germline cells in each of the two monocle3 trajectories was used for alignment using the dtw function in R package dtw. The Pearson's correlation based distance and "symmetric2" step parameters were used in dtw. The aligned time scale returned by dtw was used as the warped pseudotime. Transcript expression levels could then be plotted on the same axis, each as a proportion of its own pseudotime.

Code and Data Availability

Scripts, written in the programming languages R or Python, necessary to reproduce the analyses in this manuscript are contained in a folder hosted at: Code. Data files (.loom, .txt, .csv., .tsv, or .rds) necessary as input to the above scripts are stored at Input Files. Both the raw and the filtered data from the FCA snRNA-seq analysis are publically available as indicated in the Results section of the text. The scRNA-seq data and Moncle object are available at https://drive.google.com/drive/folders/1A2U5piOy4-HDLloFezux2dZOCGxznDQS?usp=sharing.

Acknowledgements

We especially acknowledge and thank the Fly Cell Atlas project, the Chan-Zuckerberg Biohub, the NIH sequencing facility and the laboratory of Steve Quake for the starting testis plus seminal

vesicle snRNA-seq dataset. We thank Stein Aerts and Bart Deplancke for supporting the efforts of J.J. and W.S., respectively. We acknowledge the Whitehead Institute Genome Technology Core for assistance in library preparation and sequencing of the scRNA-seq dataset, the Bloomington Drosophila Stock Center and Kyoto DGGR for *Drosophila* strains, the Developmental Studies Hybridoma Bank for various antibodies, and Aaron Allen for advice and initial code to transfer the SCope loom file format into SEURAT. S.D. thanks Dan Beiting at PennVet for his DIY_Transcriptomics course.

Funding

NIH F32 Award number 1F32GM143850-01 (Amelie Raz); Howard Hughes Medical Institute (Yukiko Yamashita); CIHR Project grant PJT-133743 (Henry Krause and Julie A. Brill); NSERC Discovery grants RGPIN-2016-06775 and RGPIN-2022-05163 (Julie A. Brill); NIH R35GM136665 and R01HD052937 (Erika Matunis); NSF 2021316576 (Jenn Viveiros); NSF 2022305201 (Jasmine Grey); NIH F31 1F31HD108918-01 (Mara Grace); NIH R35GM136433 and the Reed-Hodgson Professorship in Human Biology (Margaret Fuller); CPRIT Scholar in Cancer Research RR200063 and NIH R00AG062746 (Hongjie Li); NIH R35GM136270 (Stephen DiNardo); NIH T32 GM008216 (Gabriela Vida); NIH T32 GM007790 and a Stanford Graduate Fellowship (Sarah Stern); NIH T32 T32AR007422 (Cameron Berry); Biotechnology and Biological Sciences Research Council BB/P001564/1 (Helen White-Cooper); Brian Oliver was supported in part by the Intramural Research Program of the National Institutes of Health (NIDDK).

Competing Interests

No competing interests declared

Author Contributions

AAR, GSV, SRS, SM, JMF, JMV, SP, JRG, and MRG (‘contributed equally’) each took the lead on a particular aspect of the coding, analysis, documentation, construction of at least one specific

Figure and or its supplement, and/or assembly of supporting source data, and also re-interatively drafted sections of the narrative reporting that work. CWB led initial analysis of the testis snRNA-seq dataset and was involved in justifying the progression along the lineages. HL prepared and processed and initially analyzed the snRNA-seq samples of testis plus seminal vesicle and AAR prepared and processed and analyzed the scRNA-seq samples. JJ aided the transition from analysis in SCope to SEURAT and WAS assisted with the trajectory analyses. ZS and CH (FlyFish) designed probes and carried out *in situ* hybridizations, imaging and analysis. YY helped develop, oversee and advise on the scRNA-seq carried out by AAR. YY provided substantive guidance and advice in discussions with AAR and JF, and TP did so with SP. BO, JAB, HMK, ELM, HW-C, SD, and MTF each contributed framing of key questions, data, data interpretation, insight, and knowledge in drafting various sections of the manuscript, and/or provided images and/or code to interrogate the points considered. Virtually all authors made substantive comments impacting the direction of the work during many remote jamboree meetings, as well as commenting insightfully on the shared manuscript and Figure drafts. SD provided guidance on R and assisted with data analysis in Seurat. MTF recognized the need to communicate more than had been possible in the original FCA paper, organized the collaboration to do so, outlined figures, and wrote the first draft. Both SD and MTF helped oversee the efforts of the team, and contributed significantly to manuscript editing.

References

Alpert, A., Moore, L.S., Dubovik, T., and Shen-Orr, S.S. (2018). Alignment of single-cell trajectories to compare cellular expression dynamics. Nat. Methods *15*, 267–270.

Alphey, L., Jimenez, J., White-Cooper, H., Dawson, I., Nurse, P., and Glover, D.M. (1992). twine, a cdc25 homolog that functions in the male and female germline of Drosophila. Cell *69*, 977–988.

Amoyel, M., Sanny, J., Burel, M., and Bach, E.A. (2013). Hedgehog is required for CySC self-renewal but does not contribute to the GSC niche in the Drosophila testis. Development *140*, 56–65.

Anllo, L., and DiNardo, S. (2022). Visceral mesoderm signaling regulates assembly position and function of the Drosophila testis niche. BioRxiv 2021.09.08.459436.

Anllo, L., Plasschaert, L.W., Sui, J., and DiNardo, S. (2019). Live imaging reveals hub cell assembly and compaction dynamics during morphogenesis of the Drosophila testis niche. Dev. Biol. *446*, 102–118.

Barckmann, B., Chen, X., Kaiser, S., Jayaramaiah-Raja, S., Rathke, C., Dottermusch-Heidel, C., Fuller, M.T., and Renkawitz-Pohl, R. (2013). Three levels of regulation lead to protamine and Mst77F expression in Drosophila. Dev. Biol. *377*, 33–45.

Barreau, C., Benson, E., Gudmannsdottir, E., Newton, F., and White-Cooper, H. (2008). Post-meiotic transcription in Drosophila testes. Development *135*, 1897–1902.

Boukhatmi, H., Frendo, J.L., Enriquez, J., Crozatier, M., Dubois, L., and Vincent, A. (2012). Tup/Islet1 integrates time and position to specify muscle identity in Drosophila. Development *139*, 3572–3582.

Boyle, M., Wong, C., Rocha, M., and Jones, D.L. (2007). Decline in Self-Renewal Factors Contributes to Aging of the Stem Cell Niche in the Drosophila Testis. Cell Stem Cell *1*, 470–478.

Le Bras, S., and Van Doren, M. (2006). Development of the male germline stem cell niche in Drosophila. Dev. Biol. *294*, 92–103.

Brower, D.L., Smith, R.J., and Wilcox, M. (1981). Differentiation within the gonads of Drosophila revealed by immunofluorescence. J. Embryol. Exp. Morphol. *63*, 233–242.

Cacchiarelli, D., Qui, X., Mikkelsent, T.S., Rinn, J.L., and Trapnell, C. (2018). Aligning Single-Cell Developmental and Reprogramming Trajectories Identifies Molecular Determinants of Myogenic Reprogramming Outcome. Cell Syst. 258–268.

Cao, C., Ma, Q., Mo, S., Shu, G., Liu, Q., Ye, J., and Gui, Y. (2021). Single-Cell RNA Sequencing Defines the Regulation of Spermatogenesis by Sertoli-Cell Androgen Signaling . Front. Cell Dev. Biol. *9*.

Cao, J., Packer, J., Ramani, V., Cusanovich, D., Chau, H., Riza, D., Xiaojie, Q., Choli, L., N., F.S., J., S.F., et al. (2017). Comprehensive single-cell transcriptional profiling of a multicellular organism. Science *357*, 661–667.

Cao, J., Spielmann, M., Qiu, X., Huang, X., Ibrahim, D.M., Hill, A.J., Zhang, F., Mundlos, S., Christiansen, L., Steemers, F.J., et al. (2019). The single-cell transcriptional landscape of mammalian organogenesis. Nature *566*, 496–502.

Chandley, A.C., and Bateman, A.J. (1962). Timing of Spermatogenesis in Drosophila melanogaster using Tritiated Thymidine. Nature *193*, 299–300.

Chen, Y., Zheng, Y., Gao, Y., Lin, Z., Yang, S., Wang, T., Wang, Q., Xie, N., Hua, R., Liu, M., et al. (2018). Single-cell RNA-seq uncovers dynamic processes and critical regulators in mouse spermatogenesis. Cell Res. *28*, 879–896.

DeFalco, T., Camara, N., Le Bras, S., and Van Doren, M. (2008). Nonautonomous Sex Determination Controls Sexually Dimorphic Development of the Drosophila Gonad. Dev. Cell *14*, 275–286.

DiNardo, S., Okegbe, T., Wingert, L., Freilich, S., and Terry, N. (2011). lines and bowl affect the specification of cyst stem cells and niche cells in the Drosophila testis. Development *138*, 1687–1696.

Edgar, B.A., and O'Farrell, P.H. (1990). The three postblastoderm cell cycles of Drosophila embryogenesis are regulated in G2 by string. Cell *62*, 469–480.

Fabrizio, J.J., Boyle, M., and DiNardo, S. (2003). A somatic role for eyes absent (eya) and sine oculis (so) in drosophila spermatocyte development. Dev. Biol. *258*, 117–128.

Fairchild, M.J., Smendziuk, C.M., and Tanentzapf, G. (2015). A somatic permeability barrier around the germline is essential for Drosophila spermatogenesis. Development *142*, 268–281.

Fincher, C.T., Wurtzel, O., de Hoog, T., Kravarik, K.M., and Reddien, P.W. (2018). Cell type transcriptome atlas for the planarian Schmidtea mediterranea. Science *1736*, 1–19.

Fingerhut, J.M., and Yamashita, Y.M. (2020). mRNA localization mediates maturation of cytoplasmic cilia in Drosophila spermatogenesis. J. Cell Biol. *219*, e202003084.

Fingerhut, J.M., Moran, J. V., and Yamashita, Y.M. (2019). Satellite DNA-containing gigantic introns in a unique gene expression program during Drosophila spermatogenesis. PLoS Genet. *15*, 1–23.

Fuller, M.T. (1993). Spermatogenesis, in The Development of Drosophila (Cold Spring Harbor, NY: Cold Spring Harbor Laboratory Press).

Fuller, M.T. (1998). Genetic control of cell proliferation and differentiation in Drosophila spermatogenesis. Semin. Cell Dev. Biol. *9*, 433–444.

Fuse, N., Hirose, S., and Hayashi, S. (1994). Diploidy of Drosophila imaginal cells is maintained by a transcriptional repressor encoded by escargot. Genes Dev. *8*, 2270–2281.

Gan, Q., Chepelev, I., Wei, G., Tarayrah, L., Cui, K., Zhao, K., and Chen, X. (2010). Dynamic regulation of alternative splicing and chromatin structure in Drosophila gonads revealed by RNA-seq. Cell Res. *20*, 763–783.

1157 Ghosh-Roy, A., Kulkarni, M., Kumar, V., Shirolikar, S., and Ray, K. (2004). Cytoplasmic Dynein–
1158 Dynactin Complex Is Required for Spermatid Growth but Not Axoneme Assembly in Drosophila.
1159 Mol. Biol. Cell *15*, 2470–2483.

1160 Gönczy, P., Viswanathan, S., and DiNardo, S. (1992). Probing spermatogenesis in Drosophila
1161 with P-element enhancer detectors. Development *114*, 89–98.

1162 Gonzalez, J., Qi, H., Liu, N., and Lin, H. (2015). Piwi Is a Key Regulator of Both Somatic and
1163 Germline Stem Cells in the Drosophila Testis. Cell Rep. *12*, 150–161.

1164 Gould-Somero, M., and Holland, L. (1974). The timing of RNA synthesis for spermiogenesis in
1165 organ cultures ofDrosophila melanogaster testes. Wilhelm Roux. Arch. Entwickl. Mech. Org.
1166 *174*, 133–148.

1167 Green, C.D., Ma, Q., Manske, G.L., Shami, A.N., Zheng, X., Marini, S., Moritz, L., Sultan, C.,
1168 Gurczynski, S.J., Moore, B.B., et al. (2018). A Comprehensive Roadmap of Murine
1169 Spermatogenesis Defined by Single-Cell RNA-Seq. Dev. Cell *46*, 651-667.e10.

1170 Greenspan, L.J., de Cuevas, M., Le, K.H., Viveiros, J.M., and Matunis, E.L. (2022). Activation of
1171 the EGFR/MAPK pathway drives transdifferentiation of quiescent niche cells to stem cells in the
1172 Drosophila testis niche. Elife *11*, e70810.

1173 Guo, J., Nie, X., Giebler, M., Mlcochova, H., Wang, Y., Grow, E.J., Kim, R., Tharmalingam, M.,
1174 Matilionyte, G., Lindskog, C., et al. (2020). The Dynamic Transcriptional Cell Atlas of Testis
1175 Development during Human Puberty. Cell Stem Cell *26*, 262-276.e4.

1176 Haber, A.L., Biton, M., Rogel, N., Herbst, R.H., Shekhar, K., Smillie, C., Burgin, G., Delorey,
1177 T.M., Howitt, M.R., Katz, Y., et al. (2017). A single-cell survey of the small intestinal epithelium.
1178 Nature *551*, 333–339.

1179 Hardy, R.W., Tokuyasu, K.T., Lindsley, D.L., and Garavito, M. (1979). The germinal proliferation
1180 center in the testis of Drosophila melanogaster. J. Ultrastruct. Res. *69*, 180–190.

1181 Herrera, S.C., Sainz de la Maza, D., Grmai, L., Margolis, S., Plessel, R., Burel, M., O'Connor,
1182 M., Amoyel, M., and Bach, E.A. (2021). Proliferative stem cells maintain quiescence of their
1183 niche by secreting the Activin inhibitor Follistatin. Dev. Cell *56*, 2284-2294.e6.

1184 Hétié, P., de Cuevas, M., and Matunis, E. (2014). Conversion of Quiescent Niche Cells to
1185 Somatic Stem Cells Causes Ectopic Niche Formation in the Drosophila Testis. Cell Rep. *7*,
1186 715–721.

1187 Hof-Michel, S., and Bökel, C. (2020). Transcriptome analysis of somatic cell populations in the
1188 Drosophila testis links metabolism and stemness. BioRxiv 2020.02.24.962639.

1189 Hwa, J.J., Hiller, M.A., Fuller, M.T., and Santel, A. (2002). Differential expression of the
1190 Drosophila mitofusin genes fuzzy onions (fzo) and dmfn. Mech. Dev. *116*, 213–216.

1191 Hwa, J.J., Zhu, A.J., Hiller, M.A., Kon, C.Y., Fuller, M.T., and Santel, A. (2004). Germ-line
1192 specific variants of components of the mitochondrial outer membrane import machinery in
1193 Drosophila. FEBS Lett. *572*, 141–146.

1194 Jenkins, N.A., Kaumeyer, J.F., Young, E.M., and Raff, R.A. (1978). A test for masked message:
1195 The template activity of messenger ribonucleoprotein particles isolated from sea urchin eggs.
1196 Dev. Biol. *63*, 279–298.

1197 Kaplan, Y., Gibbs-Bar, L., Kalifa, Y., Feinstein-Rotkopf, Y., and Arama, E. (2010). Gradients of a
1198 Ubiquitin E3 Ligase Inhibitor and a Caspase Inhibitor Determine Differentiation or Death in
1199 Spermatids. Dev. Cell *19*, 160–173.

1200 Kapoor, T., Dubey, P., Shirolikar, S., and Ray, K. (2021). An actomyosin clamp assembled by
1201 the Amphiphysin-Rho1-Dia/DAAM-Rok pathway reinforces somatic cell membrane folded
1202 around spermatid heads. Cell Rep. *34*, 108918.

1203 Kawase, E., Wong, M.D., Ding, B.C., and Xie, T. (2004). Gbb/Bmp signaling is essential for
1204 maintaining germline stem cells and for repressing bam transcription in the Drosophila testis.
1205 Development *131*, 1365–1375.

1206 Kiger, A., Leanne, J.D., Cordula, S., Rogers, M., and Fuller, M. (2001). Stem Cell Self-Renewal
1207 Specified by JAK-STAT Activation in Response to a Support Cell Cue. Science *294*, 2542–
1208 2545.

1209 Kudron, M.M., Victorsen, A., Gevirtzman, L., Hillier, L.W., Fisher, W.W., Vafeados, D., Kirkey,
1210 M., Hammonds, A.S., Gersch, J., Ammouri, H., et al. (2018). The ModERN Resource: Genome-
1211 Wide Binding Profiles for Hundreds of Drosophila and Caenorhabditis elegans Transcription
1212 Factors. Genetics *208*, 937–949.

1213 Kuhn, R., Kuhn, C., Börsch, D., Glätzer, K.H., Schäfer, U., and Schäfer, M. (1991). A cluster of
1214 four genes selectively expressed in the male germ line of Drosophila melanogaster. Mech. Dev.
1215 *35*, 143–151.

1216 Law, N.C., Oatley, M.J., and Oatley, J.M. (2019). Developmental kinetics and transcriptome
1217 dynamics of stem cell specification in the spermatogenic lineage. Nat. Commun. *10*, 2787.

1218 Leatherman, J.L., and DiNardo, S. (2010). Germline self-renewal requires cyst stem cells and
1219 stat regulates niche adhesion in Drosophila testes. Nat. Cell Biol. *12*, 806–811.

1220 Li, H., Janssens, J., De Waegeneer, M., Sai, S.K., Davie, K., Gardeux, V., Saelens, W., Fabrice,
1221 D., Brbić, M., Spanier, K., et al. (2022). Fly Cell Atlas: A single-nucleus transcriptomic atlas of
1222 the adult fruit fly. Science *375*, eabk2432.

1223 Li, M.A., Alls, J.D., Avancini, R.M., Koo, K., and Godt, D. (2003). The large Maf factor Traffic
1224 Jam controls gonad morphogenesis in Drosophila. Nat. Cell Biol. *5*, 994–1000.

1225 Liu, Y., Li, J.S.S., Rodiger, J., Comjean, A., Attrill, H., Antonazzo, G., Brown, N.H., Hu, Y., and
1226 Perrimon, N. (2022). FlyPhoneDB: an integrated web-based resource for cell–cell
1227 communication prediction in Drosophila. Genetics *220*, iyab235.

1228 Lowe, N., Rees, J.S., Roote, J., Ryder, E., Armean, I.M., Johnson, G., Drummond, E., Spriggs,
1229 H., Drummond, J., Magbanua, J.P., et al. (2014). Analysis of the expression patterns,
1230 subcellular localisations and interaction partners of Drosophila proteins using a pigP protein trap
1231 library. Development *141*, 3994–4005.

1232 Lu, D., Sin, H.S., Lu, C., and Fuller, M.T. (2020). Developmental regulation of cell type-specific
1233 transcription by novel promoter-proximal sequence elements. Genes Dev. *34*, 663–677.

1234 Mahadevaraju, S., Fear, J.M., Akeju, M., Galletta, B.J., Pinheiro, M.M.L.S., Avelino, C.C.,
1235 Cabral-de-Mello, D.C., Conlon, K., Dell'Orso, S., Demere, Z., et al. (2021). Dynamic sex
1236 chromosome expression in Drosophila male germ cells. Nat. Commun. *12*, 892.

1237 McLaughlin, C.N., Brbić, M., Xie, Q., Li, T., Horns, F., Kolluru, S.S., Kebschull, J.M., Vacek, D.,
1238 Xie, A., Li, J., et al. (2021). Single-cell transcriptomes of developing and adult olfactory receptor
1239 neurons in Drosophila. Elife *10*, e63856.

1240 Michel, M., Kupinski, A.P., Raabe, I., and Bökel, C. (2012). Hh signalling is essential for somatic
1241 stem cell maintenance in the Drosophila testis niche. Development *139*, 2663–2669.

1242 Morris, C.A., Benson, E., and White-Cooper, H. (2009). Determination of gene expression
1243 patterns using in situ hybridization to Drosophila testes. Nat. Protoc. *4*, 1807–1819.

1244 Noguchi, T., Koizumi, M., and Hayashi, S. (2011). Sustained elongation of sperm tail promoted
1245 by local remodeling of giant mitochondria in Drosophila. Curr. Biol. *21*, 805–814.

1246 Okegbe, T.C., and DiNardo, S. (2011). The endoderm specifies the mesodermal niche for the
1247 germline in Drosophila via Delta-Notch signaling. Development *138*, 1259–1267.

1248 Olivieri, G., and Olivieri, A. (1965). Autoradiographic study of nucleic acid synthesis during
1249 spermatogenesis in Drosophila melanogaster. Mutat. Res. Mol. Mech. Mutagen. *2*, 366–380.

1250 Papagiannouli, F., and Mechler, B.M. (2009). discs large regulates somatic cyst cell survival and
1251 expansion in Drosophila testis. Cell Res. *19*, 1139–1149.

1252 Plass, M., Solana, J., Wolf, F.A., Ayoub, S., Misios, A., Glažar, P., Theis, F.J., Kocks, C., and
1253 Rajewsky, N. (2018). Cell type atlas and lineage tree of a whole complex animal by single-cell
1254 transcriptomics. *1723*, 1–17.

1255 Qadir, M.M.F., Álvarez-Cubela, S., Klein, D., van Dijk, J., Muñiz-Anquela, R., Moreno-
1256 Hernández, Y.B., Lanzoni, G., Sadiq, S., Navarro-Rubio, B., García, M.T., et al. (2020). Single-
1257 cell resolution analysis of the human pancreatic ductal progenitor cell niche. Proc. Natl. Acad.
1258 Sci. *117*, 10876–10887.

1259 Raja, J.S., and Renkawitz-Pohl, R. (2006). Replacement by Drosophila melanogaster
1260 Protamines and Mst77F of Histones during Chromatin Condensation in Late Spermatids and
1261 Role of Sesame in the Removal of These Proteins from the Male Pronucleus. Mol. Cell. Biol. *26*,
1262 3682.

1263 Rust, K., Byrnes, L.E., Yu, K.S., Park, J.S., Sneddon, J.B., Tward, A.D., and Nystul, T.G.
1264 (2020). A single-cell atlas and lineage analysis of the adult Drosophila ovary. Nat. Commun. *11*.

1265 Satija, R., Farrell, J.A., Gennert, D., Schier, A.F., and Regev, A. (2015). Spatial reconstruction
1266 of single-cell gene expression data. Nat. Biotechnol. *33*, 495–502.

1267 Schäfer, M., Kuhn, R., Bosse, F., and Schäfer, U. (1990). A conserved element in the leader

mediates post-meiotic translation as well as cytoplasmic polyadenylation of a Drosophila spermatocyte mRNA. EMBO (Eur. Mol. Biol. Organ.) J. *9*, 4519–4525.

Schäfer, M., Nayernia, K., Engel, W., and Schäfer, U. (1995). Translational Control in Spermatogenesis. Dev. Biol. *172*, 344–352.

Schaum, N., Karkanias, J., Neff, N.F., May, A.P., Quake, S.R., Wyss-Coray, T., Darmanis, S., Batson, J., Botvinnik, O., Chen, M.B., et al. (2018). Single-cell transcriptomics of 20 mouse organs creates a Tabula Muris. Nature *562*, 367–372.

Sebé-Pedrós, A., Saudemont, B., Chomsky, E., Plessier, F., Mailhé, M.P., Renno, J., Loe-Mie, Y., Lifshitz, A., Mukamel, Z., Schmutz, S., et al. (2018). Cnidarian Cell Type Diversity and Regulation Revealed by Whole-Organism Single-Cell RNA-Seq. Cell *173*, 1520-1534.e20.

She, M., Tang, M., Jiang, T., and Zeng, Q. (2021). The Roles of the LIM Domain Proteins in Drosophila Cardiac and Hematopoietic Morphogenesis . Front. Cardiovasc. Med. *8*.

Shi, Z., Lim, C., Tran, V., Cui, K., Zhao, K., and Chen, X. (2020). Single-cyst transcriptome analysis of Drosophila male germline stem cell lineage. Development *147*, dev184259.

Shiraiwa, T., Nitasaka, E., and Yamazaki, T. (2000). Geko, a Novel Gene Involved in Olfaction in Drosophila Melanogaster. J. Neurogenet. *14*, 145–164.

Shivdasani, A.A., and Ingham, P.W. (2003). Regulation of Stem Cell Maintenance and Transit Amplifying Cell Proliferation by TGF-β Signaling in Drosophila Spermatogenesis. Curr. Biol. *13*, 2065–2072.

Siebert, S., Farrell, J. a., Cazet, J.F., Abeykoon, Y., Primack, A.S., Schnitzler, C.E., and Juliano, C.E. (2019). Stem cell differentiation trajectories in Hydra resolved at single-cell resolution. Science *365*, 1–8.

Sitnik, J.L., Francis, C., Hens, K., Huybrechts, R., Wolfner, M.F., and Callaerts, P. (2014). Neprilysins: An Evolutionarily Conserved Family of Metalloproteases That Play Important Roles in Reproduction in Drosophila. Genetics *196*, 781–797.

Soumillon, M., Necsulea, A., Weier, M., Brawand, D., Zhang, X., Gu, H., Barthès, P., Kokkinaki, M., Nef, S., Gnirke, A., et al. (2013). Cellular Source and Mechanisms of High Transcriptome Complexity in the Mammalian Testis. Cell Rep. *3*, 2179–2190.

Susic-Jung, L., Hornbruch-Freitag, C., Kuckwa, J., Rexer, K.-H., Lammel, U., and Renkawitz-Pohl, R. (2012). Multinucleated smooth muscles and mononucleated as well as multinucleated striated muscles develop during establishment of the male reproductive organs of Drosophila melanogaster. Dev. Biol. *370*, 86–97.

Tanentzapf, G., Devenport, D., Godt, D., and Brown, N.H. (2007). Integrin-dependent anchoring of a stem-cell niche. Nat. Cell Biol. *9*, 1413–1418.

Tazuke, S.I., Schulz, C., Gilboa, L., Fogarty, M., Mahowald, A.P., Guichet, A., Ephrussi, A., Wood, C.G., Lehmann, R., and Fuller, M.T. (2002). A germline-specific gap junction protein required for survival of differentiating early germ cells. Development *129*, 2529–2539.

1305 Thor, S., and Thomas, J.B. (1997). The Drosophila islet Gene Governs Axon Pathfinding and
1306 Neurotransmitter Identity. Neuron *18*, 397–409.

1307 Tokuyasu, K.T. (1975). Dynamics of spermiogenesis in Drosophila melanogaster. VI.
1308 Significance of “onion” nebenkern formation. J. Ultrastruct. Res. *53*, 93–112.

1309 Tokuyasu, K.T., Peacock, W.J., and Hardy, R.W. (1972). Dynamics of spermiogenesis in
1310 Drosophila melanogaster. II. Coiling process. Z. Zellforsch. Mikrosk. Anat. *127*, 492–525.

1311 Trapnell, C., Cacchiarelli, D., Grimsby, J., Pokharel, P., Li, S., Morse, M., Lennon, N.J., Livak,
1312 K.J., Mikkelsen, T.S., and Rinn, J.L. (2014). The dynamics and regulators of cell fate decisions
1313 are revealed by pseudotemporal ordering of single cells. Nat. Biotechnol. *32*, 381–386.

1314 Tulina, N., and Matunis, E. (2001). Control of Stem Cell Self-Renewal in Drosophila
1315 Spermatogenesis by JAK-STAT Signaling. Science *294*, 2546–2549.

1316 Vedelek, V., Bodai, L., Grézal, G., Kovács, B., Boros, I.M., Laurinyecz, B., and Sinka, R. (2018).
1317 Analysis of Drosophila melanogaster testis transcriptome. BMC Genomics *19*, 697.

1318 Voog, J., Sandall, S.L., Hime, G.R., Resende, L.P.F., Loza-Coll, M., Aslanian, A., Yates, J.R.,
1319 Hunter, T., Fuller, M.T., and Jones, D.L. (2014). Escargot Restricts Niche Cell to Stem Cell
1320 Conversion in the Drosophila Testis. Cell Rep. *7*, 722–734.

1321 Wasbrough, E.R., Dorus, S., Hester, S., Howard-Murkin, J., Lilley, K., Wilkin, E., Polpitiya, A.,
1322 Petritis, K., and Karr, T.L. (2010). The Drosophila melanogaster sperm proteome-II (DmSP-II).
1323 J. Proteomics *73*, 2171–2185.

1324 Wendt, G., Zhao, L., Chen, R., Liu, C., O’Donoghue, A., Caffrey, C., Reese, M., and Collins, J.
1325 (2020). A single-cell RNA-seq atlas of Schistosoma mansoni identifies a key regulator of blood
1326 feeding. Science *369*, 1644–1649.

1327 White-Cooper, H., Schafer, M.A., Alphey, L.S., and Fuller, M.T. (1998). Transcriptional and
1328 post-transcriptional control mechanisms coordinate the onset of spermatid differentiation with
1329 meiosis I in Drosophila. Development *125*, 125–134.

1330 Wilk, R., Hu, J., and Krause, H.M. (2017). In Situ Hybridization: Fruit Fly Embryos and Tissues.
1331 Curr. Protoc. Essent. Lab. Tech. *15*, 9.3.1-9.3.26.

1332 Witt, E., Benjamin, S., Svetec, N., and Zhao, L. (2019). Testis single-cell RNA-seq reveals the
1333 dynamics of de novo gene transcription and germline mutational bias in drosophila. Elife *8*, 1–
1334 22.

1335 Zoller, R., and Schulz, C. (2012). The Drosophila cyst stem cell lineage. Spermatogenesis *2*,
1336 145–157.

1337

1338